
[All ETDs from UAB](#)

[UAB Theses & Dissertations](#)

1994

An Analysis Of Constitutional Liquid Film Migration In The Nickel-Base Alloy 718.

Viola Lenora Acoff
University of Alabama at Birmingham

Follow this and additional works at: <https://digitalcommons.library.uab.edu/etd-collection>

Recommended Citation

Acoff, Viola Lenora, "An Analysis Of Constitutional Liquid Film Migration In The Nickel-Base Alloy 718." (1994). *All ETDs from UAB*. 4708.
<https://digitalcommons.library.uab.edu/etd-collection/4708>

This content has been accepted for inclusion by an authorized administrator of the UAB Digital Commons, and is provided as a free open access item. All inquiries regarding this item or the UAB Digital Commons should be directed to the [UAB Libraries Office of Scholarly Communication](#).

INFORMATION TO USERS

This manuscript has been reproduced from the microfilm master. UMI films the text directly from the original or copy submitted. Thus, some thesis and dissertation copies are in typewriter face, while others may be from any type of computer printer.

The quality of this reproduction is dependent upon the quality of the copy submitted. Broken or indistinct print, colored or poor quality illustrations and photographs, print bleedthrough, substandard margins, and improper alignment can adversely affect reproduction.

In the unlikely event that the author did not send UMI a complete manuscript and there are missing pages, these will be noted. Also, if unauthorized copyright material had to be removed, a note will indicate the deletion.

Oversize materials (e.g., maps, drawings, charts) are reproduced by sectioning the original, beginning at the upper left-hand corner and continuing from left to right in equal sections with small overlaps. Each original is also photographed in one exposure and is included in reduced form at the back of the book.

Photographs included in the original manuscript have been reproduced xerographically in this copy. Higher quality 6" x 9" black and white photographic prints are available for any photographs or illustrations appearing in this copy for an additional charge. Contact UMI directly to order.

UMI

A Bell & Howell Information Company
300 North Zeeb Road, Ann Arbor, MI 48106-1346 USA
313/761-4700 800/521-0600

Order Number 9520548

**An analysis of constitutional liquid film migration in the
nickel-base alloy 718**

Acoff, Viola Lenora, Ph.D.

University of Alabama at Birmingham, 1994

U·M·I

**300 N. Zeeb Rd.
Ann Arbor, MI 48106**

AN ANALYSIS OF CONSTITUTIONAL LIQUID FILM MIGRATION IN THE
NICKEL-BASE ALLOY 718

by

VIOLA L. ACOFF

A DISSERTATION

Submitted in partial fulfillment of the requirements for
the degree of Doctor of Philosophy in the Department of
Materials Science and Engineering in the Graduate School,
The University of Alabama at Birmingham

BIRMINGHAM, ALABAMA

1994

ABSTRACT OF DISSERTATION
GRADUATE SCHOOL, UNIVERSITY OF ALABAMA AT BIRMINGHAM

Degree Doctor of Philosophy Major Subject Materials Engineering
Name of Candidate Viola L. Acoff
Title An Analysis of Constitutional Liquid Film Migration
In The Nickel-Base Alloy 718

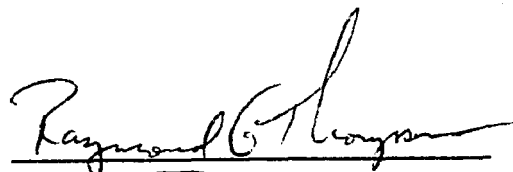
When multiphase alloys are rapidly heated it is possible to cause melting of the interface between phases. This is called constitutional liquation if, during melting, the bulk composition is in a non-liquid region of the phase diagram but the tie-line between the liquating phases passes through a liquid region. The liquid produced during constitutional liquation can spread along grain boundaries and promote liquid film migration (LFM). This is known as constitutional liquid film migration (CLFM). CLFM is thermodynamically similar to liquid film migration; however, mechanistically there are significant differences.

Nickel-base alloy 718 has been studied to show the features of migration which are unique to CLFM. Experimentation consisted of heat treating rods of alloy 718 to promote the trapping of niobium carbide particles on the grain boundaries. These samples were then subjected to isothermal treatments above their constitutional liquation


temperature which produced CLFM of the grain boundaries. The movement of the grain boundaries away from their centers of curvature, the formation of a new solid solution behind the migrated boundaries, and the reversals of curvature of the migrated grain boundaries confirmed that CLFM was the phenomenon observed.

Niobium enrichment occurred in the region behind the migrated grain boundaries for isothermal treatments below the solidus temperature whereas no niobium enrichment occurred for isothermal treatment above the solidus temperature. The rate of migration was shown to increase only slightly with increasing temperature. The suppression of CLFM at 1260°C was explained by a criterion for predicting coherency breaking in the region located in front of the migrating grain boundary. The validity of the coherency strain hypothesis as the driving force for CLFM in alloy 718 is also discussed.

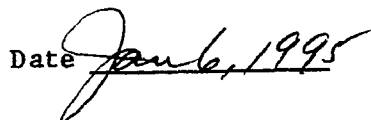
Abstract Approved by: Committee Chairman



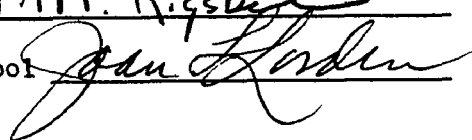
Program Director



Date



Dean of Graduate School



DEDICATION

This dissertation is dedicated to the memory of my mother, Mary Lester Winfield Acoff. Although you were not here physically during the last four months for the completion of this work, I still could hear your comforting words of encouragement that always helped me make it through difficult times. Mother, your perseverance and nurturing made this achievement possible and I am forever grateful that I was blessed to have a mother like you.

Thanks

ACKNOWLEDGEMENTS

My sincere thanks go to my advisor, Dr. Raymond G. Thompson, for his guidance throughout the duration of my undergraduate and graduate studies at UAB. Thanks for everything.

I also would like to thank my committee members, Drs. Robin D. Griffin, J. Barry Andrews, Burton R. Patterson, and John Barnard. Your input and assistance were invaluable and greatly appreciated.

Finally, I would like to thank my father, Mr. Roosevelt Acoff, Sr., and all of my sisters and brothers, Linda, Leslie, Carl Sr., Alfredo, Cassandra, Roosevelt Jr., Sharon, and Valerie, for their endless support and encouragement.

TABLE OF CONTENTS

	<u>Page</u>
ABSTRACT	ii
DEDICATION	iv
ACKNOWLEDGEMENTS	v
LIST OF TABLES	viii
LIST OF FIGURES	ix
INTRODUCTION	1
A. Liquid Film Migration	1
B. Constitutional Liquid Film Migration	6
C. Theory of Niobium Segregation	12
D. Objectives	16
EXPERIMENTAL PROCEDURE	17
A. Material	17
B. Heat Treatment	17
C. Isothermal Treatments	19
D. Light Microscopy	20
E. Determination of Migration Rates	21
F. EBSD System Analysis	23
G. Transmission Electron Microscopy	27
H. Auger Electron Microscopy	33
RESULTS	34
A. As-Received Condition	34
B. As-Heat Treated Condition	34
C. 1227 °C Isothermal Treatment	34
D. 1240 °C Isothermal Treatment	42
E. 1250 °C Isothermal Treatment	55

TABLE OF CONTENTS (Continued)

	<u>Page</u>
F. 1260 °C Isothermal Treatment	61
G. Auger Electron Analysis	61
H. Migration Rates	65
I. Niobium Diffusivity	65
 DISCUSSION	 69
A. Confirmation of Constitutional Liquid Film Migration	 69
1. Movement Away from Center of Curvature	69
2. Formation of a New Solid Solution	69
3. Reversal of Curvature	70
4. Difficulty in Confirming CLFM	72
5. Similar Features of CLFM and DIGM	72
B. Niobium Concentration Versus Temperature	74
C. Migration Rate Versus Temperature	84
D. Influence of Crystal Orientation on CLFM	88
 SUMMARY	 90
 CONCLUSIONS	 91
 LIST OF REFERENCES	 92
 APPENDIX	 95

LIST OF TABLES

<u>Table</u>	<u>Page</u>
I Composition of Alloy 718 in Weight Percent . .	18
II Measured Migration Distance Data for 1227°C	24
III Measured Migration Distance Data for 1240°C	25
IV Measured Migration Distance Data for 1250°C	26
V Characterization of Migrated Grain Boundaries	45
VI Average Migration Distances and Migration Rates	66
VII Diffusivity of Niobium in the Matrix	68
VIII Data for Construction of γ -NbC Pseudo-Binary Phase Diagram	79
IX Diffusivity/Migration Rate (D/MR) Values . . .	86

LIST OF FIGURES

Figure	Page
1	Free energy versus composition diagrams for liquid film in contact with matrix. C_s and C_L are the compositions of the matrix and the liquid, respectively, in the absence of coherency stress in the matrix. C'_s and C'_L are the altered compositions due to the presence of coherency stress in the matrix (Ref. 9) 4
2	Concentration gradient which occurs in a grain boundary liquid film due to the presence of coherency strains at the solid-liquid interface. K_1 and K_2 are the orientation dependent modulus of grain 1 and grain 2, respectively (Ref. 15) 7
3	Schematic of constitutional liquation of particle AB in a binary alloy C_0 (Ref. 15) 9
4	Schematic of the formation of a lateral concentration gradient in the grain boundary liquid film due to the constitutional liquation of AB particles (Ref. 15) 13
5	Approximate γ -NbC pseudo-binary phase diagram for alloy 718 15
6	Relationship between σ_A (apparent migration distance) and σ_T (true migration distance) shown schematically 22

LIST OF FIGURES (continued)

<u>Figure</u>		<u>Page</u>
7	Sketch showing how samples were sectioned and mounted for TEM specimen preparation . . .	30
8	Light micrograph of as-received condition of alloy 718. Microstructure consists of carbides and Ni_3Nb (δ phase) in the γ matrix	35
9	Light microscope image showing the microstructure of alloy 718 after the 650°C for 4 hours heat treatment. The arrows point to niobium carbides on the grain boundaries	36
10	(a) Light micrograph and (b) SEM micrograph of 1227°C peak temperature sample showing the original grain boundary position (OGB) and a grain boundary with reversed curvature as a result of CLFM (CLFM)	38
11	TEM bright-field image of 1227°C peak temperature sample showing area where TEM/EDS profiles were obtained	39
12	Representative TEM/EDS spectra from the a) matrix and b) migrated region of the 1227°C peak temperature sample	40
13	Niobium concentration versus distance profile for the 1227°C sample	41
14	Representative SEM micrograph of typical areas where orientation analysis was performed for the 1227°C peak temperature sample. The migrated grain boundary is denoted by CLFM. The image was taken using the approximately 70° tilt necessary for EBSD analysis	43

LIST OF FIGURES (Continued)

<u>Figure</u>	<u>Page</u>
15	EBSP patterns from two alloy 718 grains that were separated by a CLFM grain boundary 44
16	Light micrograph of 1240°C peak temperature sample showing the original grain boundary position (OGB) and a grain boundary with reversed curvature as a result of CLFM (CLFM) 46
17	(a) TEM bright-field image showing area where TEM/EDS profiles were obtained for the 1240°C peak temperature sample. (b) SEM secondary electron image of an area (boxed region) that is similar to the TEM image shown in (a) 48
18	Representative TEM/EDS spectra from the a) matrix and b) migrated region of the 1240°C peak temperature sample 49
19	Niobium concentration versus distance profile for 1240°C collected along data line 1 shown in Figure 17a 50
20	Niobium concentration versus distance profile for 1240°C collected along data line 2 shown in Figure 17a 51
21	Niobium concentration versus distance profile for 1240°C collected along data line 3 shown in Figure 17a 52
22	(a) Light micrograph and (b) SEM micrograph of 1250°C peak temperature sample showing the original grain boundary position (OGB) and a grain boundary with reversed curvature as a result of CLFM (CLFM) 56

LIST OF FIGURES (Continued)

<u>Figure</u>		<u>Page</u>
23	TEM bright-field image showing area where TEM/EDS profiles were obtained for the 1250°C peak temperature sample	58
24	Representative TEM/EDS spectra from the a) matrix and b) migrated region of the 1250°C peak temperature sample	59
25	Niobium concentration versus distance profile for 1250°C	60
26	(a) Light micrograph and (b) SEM secondary electron image of alloy 718 for the 1260°C peak temperature sample	62
27	Auger spectrum from the migrated region of the 1227°C sample	63
28	Auger spectrum from the matrix of the 1227°C sample	64
29	Migration rate plotted as a function of temperature	67
30	Approximate γ -NbC pseudo-binary phase diagram showing compositions of niobium for 1227°C, 1240°C, and 1250°C	76

INTRODUCTION

A. Liquid Film Migration

Researchers have shown that it is possible to cause grain boundaries to migrate as a result of solute atoms diffusing along the grain boundaries (1,2,3,4). This phenomenon has been termed diffusion induced grain boundary migration (DIGM). Microstructural features which distinguished DIGM from curvature driven migration were that the grain boundaries often moved away from their centers of curvature and a new solid solution formed behind the migrating boundaries (5). Similar migration characteristics may occur when the grain boundary is replaced by a liquid film. Liquid film migration (LFM) can be qualitatively considered as a variant of the DIGM process and has been shown to exhibit some of the same microstructural features as DIGM (6,7).

LFM was first observed in liquid phase sintering experiments. Some of the studies which set the basis for LFM experiments were done by Yoon and Huppmann (6) and Song et al. (7). Yoon and Huppmann sintered tungsten particles in liquid nickel and showed that films of liquid nickel between tungsten

grains migrated by dissolving a tungsten grain on one side and depositing an equilibrium W-Ni alloy on the other. Song et al. sintered compacts of tungsten and nickel powders. The sintered W-Ni specimens were resintered after placing compacts of iron powders on them. The liquid films between the grains were observed to migrate by dissolving the W-Ni grains and reprecipitating W-Ni-Fe solid. The authors concluded that liquid films in binary alloys prepared by liquid phase sintering migrated when a third solute was added to form ternary solutions.

Several hypotheses have been proposed for the driving force for LFM. However, the hypothesis which explains many of the experimental observations by previous researchers is the coherency strain hypothesis (8). Handwerker (9) expressed the coherency strain energy for cubic crystals as

$$f_{\text{COHERENT}} = Y(n) \delta^2$$

where $Y(n)$ is an orientation-dependent elastic modulus and δ is the coherency strain that is defined as

$$\delta = (a - a_0) / a_0$$

where a and a_0 are the lattice parameters of the matrix at the solid-liquid interface and the grain interior, respectively.

For elastic isotropy (no variation with orientation) $Y(n)$ reduces to

$$Y = E/(1-\nu)$$

where E is Young's modulus and ν is Poisson's ratio.

According to the coherency strain hypothesis, when a solute-rich liquid comes into contact with the solid matrix, the solute atoms will diffuse into the matrix and cause a coherency strain due to the difference in size between the matrix and solute atoms. This strain causes a shift in the free energy curve for the liquid-matrix interface on that side of the film where coherency persists (Figure 1). This shift in the free energy curve can be described by first considering the free energy versus composition diagram for an alloy. The minimum free energy, i.e. the equilibrium state, is denoted as the lowest point on the free energy curve. Porter and Easterling (10) stated that the free energy rises due to the presence of surfaces, grain boundaries, and dislocations. Porter and Easterling (11) also suggested that the formation of coherent interfaces raise the free energy of a system due to the elastic strain fields that arise.

Hillert (12) also postulated that the free energy curve rises when coherency stresses are present. He showed that the increase in free energy due to the presence of coherency

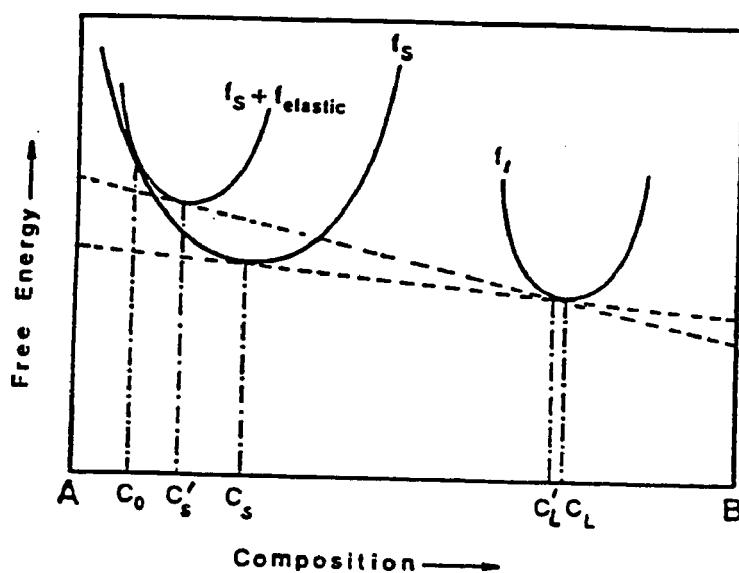


Figure 1. Free energy versus composition diagrams for liquid film in contact with matrix. C_s and C_L are the compositions of the matrix and the liquid, respectively, in the absence of coherency stress in the matrix. C'_s and C'_L are the altered compositions due to the presence of coherency stress in the matrix (Ref. 9).

stresses offset the free energy loss due to volume diffusion which resulted in a net increase in total free energy. Hillert attributed the increased free energy to the elastic energy which arises when coherency stresses are present. This explains why the free energy curves shift when coherency strains are present as shown in Figure 1. The curve is tied to the composition of the matrix that joins the liquid at the time the liquid film originates.

LFM is caused by a transverse composition gradient in the liquid film which occurs as a result of the effect of coherency strain on the free energy curve. This can be shown by Figure 1 (9). The equilibrium compositions of the solid and liquid in the absence of coherency strain are denoted by C_s and C_L , respectively. When coherency strain is present in the matrix, the free energy curve for the solid moves up while the free energy curve for the liquid remains the same. This results in the equilibrium compositions of the solid and liquid being altered to C'_s and C'_L , respectively. Figure 1 also shows that the solute concentration in the liquid decreases in the presence of coherency strain.

The coherency strain in the matrix at the solid - liquid (S-L) interface is directly proportional to the orientation dependent elastic modulus for a given solute (14). Therefore,

the coherency strains at the S-L interface on either side of the boundary will be unequal due to the orientation mismatch across the grain boundary. Consider two grains separated by grain boundary liquid where grain 2 has a greater coherency strain than grain 1 due to the orientation dependent modulus (K) for grain 2 being greater (Figure 2) (15). The liquid in contact with grain 2 will be more deplete in solute than the liquid in contact with grain 1. This results in a concentration gradient across the grain boundary liquid (denoted as ΔC in Figure 2) and leads to diffusion of solute across the liquid film towards grain 2 according to Fick's first law. Thus, migration of the liquid film occurs in the direction of grain 2. In the absence of coherency strain, there will be no concentration gradient across the liquid film and thus no migration (9,15).

B. Constitutional Liquid Film Migration

Previous researchers (5,6,7,16-22) did not observe LFM to occur in situ. Radhakrishnan and Thompson were the first to report LFM occurring in situ in the weld heat affected zone (HAZ) of alloy 718 as a result of constitutional liquation (23). Radhakrishnan and Thompson (24) also showed that LFM and subgrain coalescence explain most of the observed microstructural phenomena and the kinetics of grain growth in

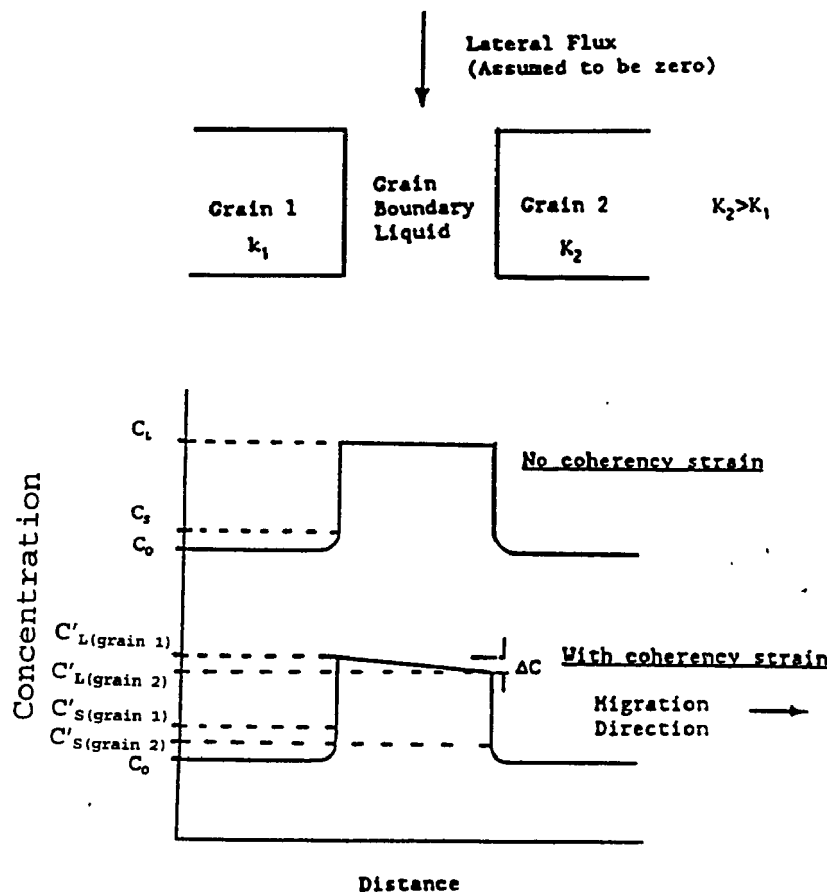


Figure 2. Concentration gradient which occurs in a grain boundary liquid film due to the presence of coherency strains at the solid - liquid interface. K_1 and K_2 are the orientation dependent modulus of grain 1 and grain 2, respectively (Ref. 15).

alloy 718. Nakkalil et al. later reported LFM from constitutional liquation in the HAZ of INCOLOY 903 (25). Nakkalil et al. (26), following the suggestion of Radhakrishnan and Thompson (23), also showed that HAZ microfissuring in INCOLOY 903 is minimized if the liquid films on the HAZ grain boundaries can partially equilibrate by LFM instead of by normal solidification.

Constitutional liquation can be best described in terms of a binary alloy. Consider a binary alloy with a phase diagram like the one shown in Figure 3. If an alloy with composition C_0 is rapidly heated above its eutectic temperature (T_E) to a temperature T , the AB particles will not have sufficient time to dissolve. Therefore, a diffusion couple is set up between the AB particles and the matrix which have the compositions of C_{AB} and C_M , respectively (Figure 3a). In front of the AB particles, liquid forms in accordance with the phase diagram and has a composition which ranges from C_{L1} to C_{L2} (Figure 3b). The situation in Figure 3c eventually occurs and the liquid which came from the liquating AB particles spreads along the grain boundaries due to particles located on the grain boundaries or particles intercepted by moving grain boundaries. The liquid would thus be present as grain boundary films.

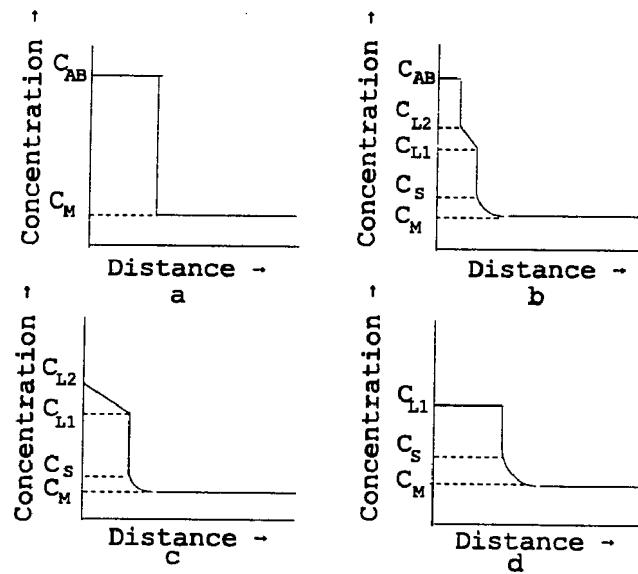
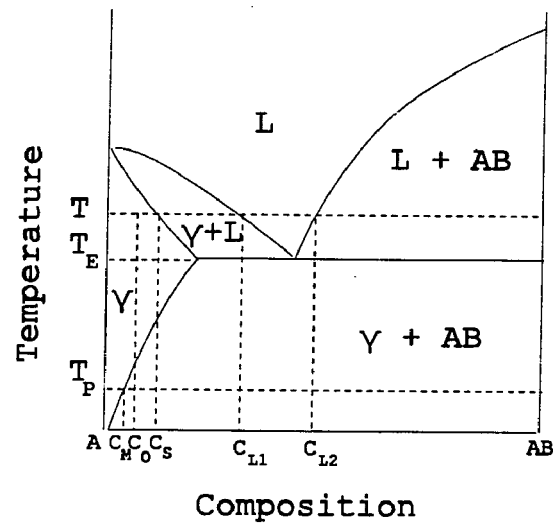


Figure 3. Schematic of constitutional liquation of particle AB in a binary alloy C_0 (Ref. 15).

Since the AB particles would not be present under equilibrium conditions, the liquid which forms from liquating AB particles is metastable. Thus, the liquid would eventually disappear due to back-diffusion of solute into the matrix (27). The back-diffusion of solute atoms from the liquid to the matrix could cause coherency strain to develop if there is a size difference between the solute and matrix atoms. This could promote the migration of grain boundaries (23). Since the concentration gradient in the liquid is metastable, it will eventually disappear and the situation in Figure 3d will occur.

The free energy theory shown in Figure 1 also applies to the non-equilibrium occurrence of LFM as a result of constitutional liquation. Figure 2 also applies here with one exception. The lateral flux is not assumed to be zero since there is a lateral flux of solutes along the liquid film which is driven by the metastable concentration gradient that exists in the liquid film. That is, there is a concentration gradient in the plane parallel to the grain boundary and also a concentration gradient in the plane perpendicular to the grain boundary. The presence of a lateral flux in the liquid (Figure 2) would result in the migration velocity reaching a steady state value (28). The steady state value was determined by the

condition that the lateral solute flux is equal to the solute flux transferred across the migrating liquid film in growing the solute-rich grain. The steady state velocity was shown to be (28),

$$v = \frac{12\sigma D_L}{5L^2} \left(\frac{4C_o}{C_L \bar{k}_L} - 1 \right)$$

where σ is the solid-liquid interfacial energy, D_L is the diffusion coefficient for solute in the liquid, L is the length of the liquid film, C_o is the solute concentration of the matrix in the growing grain, C_L is the solute concentration in the liquid at the trailing interface, and \bar{k} is the average curvature of the liquid film.

The phenomenon described above which causes grain boundaries to migrate as a result of the formation of a metastable grain boundary liquid has been termed constitutional liquid film migration (CLFM). CLFM is thermodynamically similar to LFM; however, mechanistically there are some significant differences. Features that are unique to CLFM are as follows:

- 1) The metastable grain boundary liquid film results from the spreading of liquid which forms from the constitutional liquation of precipitates located on the

grain boundaries.

2) A lateral diffusion flux of solutes occurs along the liquid film. This is due to the lateral concentration gradient which arises when the liquid, formed from individual particles, coalesce to form the grain boundary film. The result is a lateral concentration gradient in the grain boundary films which ranges from C_{L1} to C_{L2} as shown in Figures 3c and 4 (15). This lateral concentration gradient is in addition to the curvature dependent lateral concentration gradient described by Brechet and Purdy (28).

CLFM, as observed by the present author (29) and by others (23, 25), originated from discrete precipitates which produce in-plane solute flux as found in DIGM and as necessary to operate the Brechet and Purdy (28) model for LFM. This suggests that flux in the plane of the liquid film is a possible mechanism for the driving force for CLFM. Therefore, CLFM could come from either coherent strain or from in-plane solute flux.

C. Theory of Niobium Segregation

Radhakrishnan and Thompson (23) showed that there is niobium enrichment behind the migrated boundaries in alloy 718 for specimens treated isothermally at 1200°C. Results from

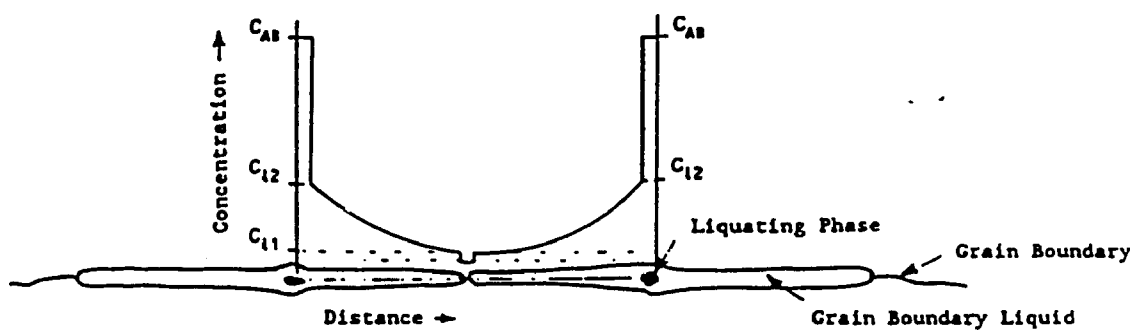


Figure 4. Schematic of the formation of a lateral concentration gradient in the grain boundary liquid film due to the constitutional liquation of AB particles (Ref. 15).

work conducted in the present study show that niobium enrichment also occurs behind the migrated boundaries in alloy 718 at an isothermal treatment of 1227°C. The exact γ matrix solidus temperature for alloy 718 is not known. The γ solidus temperature (T_s) for alloy 718 was shown to range from 1227°C to 1235°C by Radhakrishnan and Thompson (30). Knorovsky et al. (31) showed that T_s ranges from 1232°C to 1260°C. The theory proposed for this study is that there will be a reversal in niobium segregation behind the migrated boundaries in alloy 718 when the peak temperature is increased above the solidus temperature.

This theory was based on the solidus curve for the γ -NbC binary phase diagram. The approximate γ -NbC pseudo-binary phase diagram shown in Figure 5 was determined from data obtained from work by Radhakrishnan and Thompson (27), Knorovsky et al. (31), and Eiselstein (32). The composition of the alloy used in the present study is denoted on the phase diagram by C_0 . If alloy C_0 is rapidly heated to temperature T_1 that is above the eutectic temperature (T_E) but below the solidus temperature, the niobium concentration in the migrated region is denoted by C_{T_1} . However, if alloy C_0 is rapidly heated to temperature T_2 that is above the solidus temperature, the niobium concentration in the migrated region

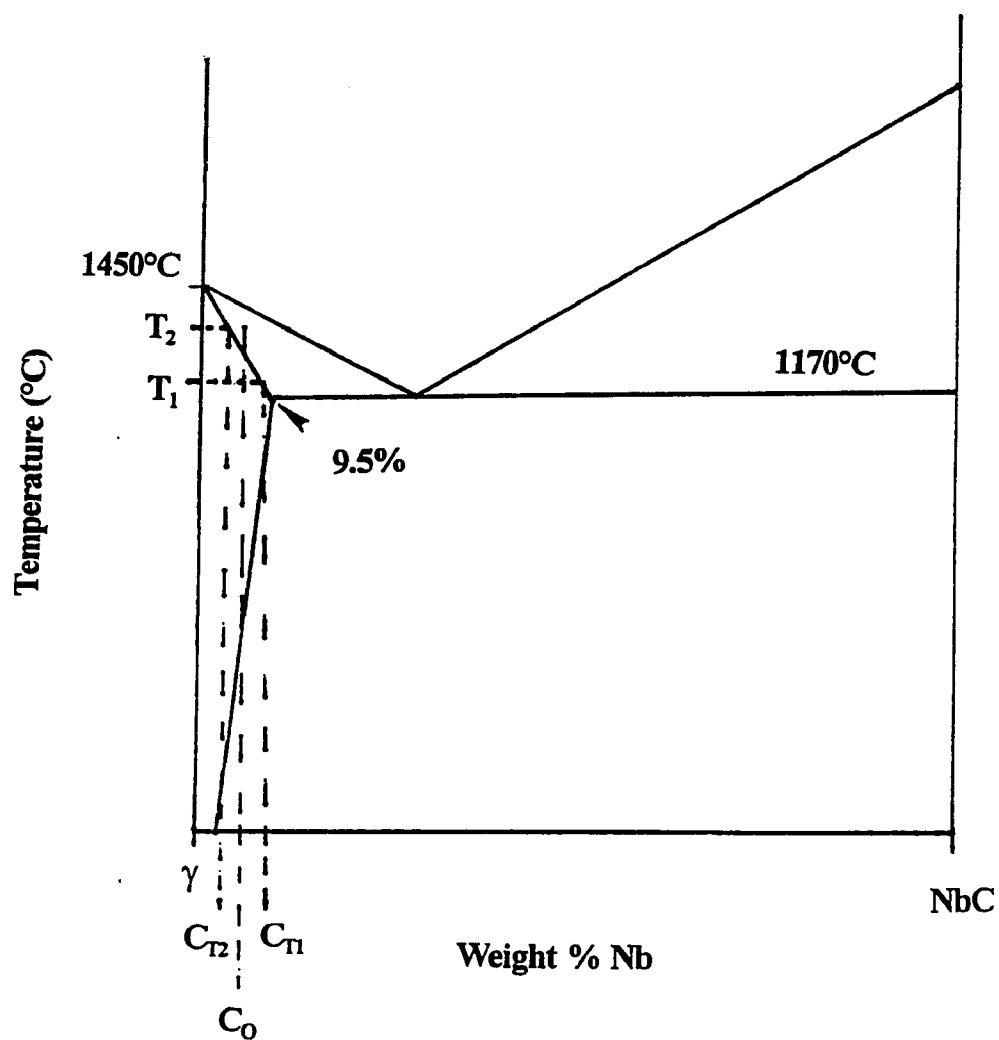


Figure 5. Approximate γ -NbC pseudo-binary phase diagram for alloy 718.

is denoted by C_{T_2} . Thus, the niobium segregation behind the migrated boundaries should follow the slope of the solidus curve and decrease from C_{T_1} to C_{T_2} when the temperature is raised above the solidus temperature.

D. Objectives

Since LFM was observed to occur in situ in the weld HAZ of multiphase alloys due to constitutional liquation, it is important that this phenomenon be fully understood. To date, there has been no systematic investigations of CLFM. It is the purpose of this study to investigate LFM accompanying constitutional liquation in alloy 718 in order to gain a better understanding of the conditions under which this phenomenon occurs. The objectives are:

- 1) Confirm that CLFM was the phenomenon observed.
- 2) Determine the effect of increasing the temperature above the solidus temperature of alloy 718 on Nb segregation behind the migrated boundaries.
- 3) Determine the migration rate as a function of peak temperature.
- 4) Determine the influence of crystal orientation on CLFM.

EXPERIMENTAL PROCEDURE

A. Material

Alloy 718 is a nickel-base superalloy which mainly consists of an FCC solid solution of nickel, iron, and chromium with a significant amount of molybdenum and niobium. The alloy 718 used in this study was received in the solution treated condition. This treatment consisted of holding the material at 954°C (1750°F) for 1 hour then water quenching. This was followed by holding at 718°C (1325°F) for 8 hours then furnace cooling to 621°C (1150°F) and holding for 8 hours. The material was then air cooled to room temperature. The material was in the form of a hot-rolled rod, 1.295cm (0.510in.) in diameter that was cut into samples approximately 10.16cm (4in.) in length. The composition of the alloy is shown in Table I.

B. Heat Treatment

The samples were placed inside stainless steel bags and solutionized in a furnace at 1093°C for 30 minutes followed by water quenching. The samples were then placed in a furnace at 650°C where they were held for 4 hours followed by air

Table I. Composition of Alloy 718 in Weight Percent

Ni	52.44
Cr	18.23
Fe	19.06
Nb+Ta	5.05
Mo	3.01
Ti	1.00
Al	0.55
Co	0.26
Si	0.12
Mn	0.11
C	0.055
S	0.003
P	0.008
Cu	0.05
B	0.0037

cooling. The 650°C heat treatment was used to promote the trapping of niobium carbide particles on the grain boundaries. The heat treated samples were sanded with silicon carbide paper to remove the thin oxidation layer which formed on the surface during heat treatment.

C. Isothermal Treatments

A Type K thermocouple was percussion welded to the midsection of the samples. In order to promote CLFM, the samples were subjected to rapid thermal cycles (recorded by the thermocouples) using a Gleeble 1000 thermomechanical device. Samples were heated at 100°C per second to a peak temperature of 1227°C and held isothermally for 4 seconds followed by water quenching. This procedure was repeated for different samples using peak temperatures of 1240°C, 1250°C, and 1260°C. After the CLFM thermal treatments, the samples were sectioned at the location of the control thermocouple and one part was used for analysis on a JEOL JEM-2000FX transmission electron microscope (TEM) and the other was used for analysis on a light microscope and a Philips 515 scanning electron microscope (SEM).

The Gleeble was calibrated 3 months after the samples for this study were submitted to rapid thermal cycles. The actual temperature was 10°C higher than the temperature that was set

in the heat-up program and read by the control thermocouples. Other samples were run on the Gleeble after the samples in the present study and before calibration of the Gleeble. These samples were set to run at a peak temperature of 1227°C but the microstructure looked more like the 1240°C samples in the present study. The exact error in temperature for the present study is not known but the appearance of the microstructures was used to determine whether the temperature was below or above the solidus temperature. If there was evidence of melting in the matrix, the temperature was determined to be above the solidus temperature. If there was no evidence of melting in the matrix, the temperature was determined to be below the solidus temperature.

D. Light Microscopy

Samples were prepared for light microscopy by mounting in bakelite and grinding on silicon carbide paper from 240-grit through 600-grit. The samples were then polished on nylon cloth using 6, 3, and 1-micron diamond paste. Etching was performed electrolytically using 10% oxalic acid. The conditions were 6 volts and 25 seconds. This procedure was used for the as-received and as-heat treated conditions and also for the 1227°C, 1240°C, 1250°C, and 1260°C isothermal treatments.

Light microscopy was used to determine the relative distances between the migrated boundaries and the original boundary positions. This information was useful for finding the migrated boundaries in the TEM specimens. Light microscopy was also used to determine the migration rates.

E. Determination of Migration Rates

Light micrographs taken at a magnification of 500X were used to determine the migration rates. The migration rates were determined by measuring the distance between the original grain boundary position and the migrated grain boundary. This was accomplished by placing a ruler on the micrographs and measuring the distance between the original grain boundary position and the migrated grain boundaries which exhibited reversals of curvature. The measured length was divided by the magnification, 500X. The measured migrated distances were actually the apparent migration distance (σ_A). The relationship between σ_A and σ_T (true migration distance) is shown schematically in Figure 6. Patterson (33) derived the following equation which shows how σ_T can be determined from σ_A (the complete derivation is shown in Appendix A)

$$\sigma_T = \frac{2}{\pi} \left(\frac{1}{\left(\frac{1}{\sigma_A} \right)} \right) = 0.64 \left(\frac{1}{\left(\frac{1}{\sigma_A} \right)} \right)$$

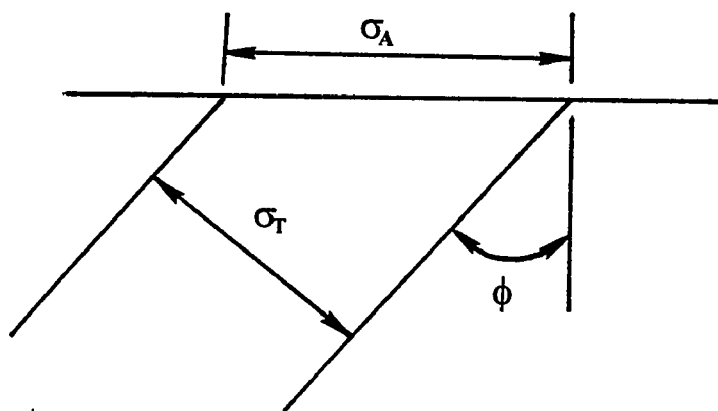


Figure 6. Relationship between σ_A (apparent migration distance) and σ_T (true migration distance) shown schematically.

There were 12 measured apparent migration distances, σ_A , for 1227°C, 9 for 1240°C, and 15 for 1250°C. These values are shown in Tables II, III, and IV, for 1227°C, 1240°C, and 1250°C, respectively. Tables II, III, and IV also show the values for $\sigma_A/500X$ and $1/\sigma_A$. The averages of the $1/\sigma_A$ values were determined for each temperature and substituted into the equation for σ_T to determine the true migration distance for each temperature. Each true migration distance was divided by 4 seconds, the time held at the peak temperature, to determine the migration rate.

The standard deviation of the $1/\sigma_A$ values was determined. The standard deviation was then added to the average $1/\sigma_A$ value then substituted into the equation for σ_T . This σ_T value was divided by 4 seconds to determine the lower limit of the migration rate. The upper limit of the migration rate was found similarly by subtracting the standard deviation of $1/\sigma_A$ from the average value of $1/\sigma_A$. This procedure was performed for 1227°C, 1240°C, and 1250°C.

F. EBSP System Analysis

Metallographic preparation for evaluation on a SEM equipped with an electron backscatter pattern system (EBSP) was different from the procedure used for light microscopy. Sample preparation consisted of grinding from 240-grit through

Table II. Measured Migration Distance Data for 1227°C

Observation Number	σ_A (mm)	$\sigma_A/500X$ (μm)	$1/\sigma_A$ ($1/\mu\text{m}$)
1	4.0	8	0.125
2	3.5	7	0.143
3	4.0	8	0.125
4	8.0	16	0.063
5	7.0	14	0.071
6	5.0	10	0.100
7	4.0	8	0.125
8	5.0	10	0.100
9	4.5	9	0.111
10	8.5	17	0.059
11	8.5	17	0.059
12	5.0	10	0.100

Table III. Measured Migration Distance Data for 1240°C

Observation Number	σ_A (mm)	$\sigma_A/500X$ (μm)	$1/\sigma_A$ ($1/\mu\text{m}$)
1	7.0	14	0.071
2	4.0	8	0.125
3	8.0	16	0.063
4	6.0	12	0.083
5	6.0	12	0.083
6	4.0	8	0.125
7	4.0	8	0.125
8	6.0	12	0.083
9	10.0	20	0.050

Table IV. Measured Migration Distance Data for 1250°C

Observation Number	σ_A (mm)	$\sigma_A/500X$ (μm)	$1/\sigma_A$ ($1/\mu\text{m}$)
1	5.0	10	0.100
2	6.0	12	0.083
3	4.0	8	0.125
4	4.5	9	0.111
5	4.5	9	0.111
6	6.0	12	0.083
7	7.0	14	0.071
8	8.0	16	0.063
9	9.5	19	0.053
10	6.0	12	0.083
11	5.5	11	0.091
12	6.5	13	0.077
13	5.5	11	0.091
14	5.5	11	0.091
15	5.0	10	0.100

600-grit silicon carbide followed by polishing with 6-micron diamond paste. The samples were removed from the bakelite mount and electrolytically polished for 60 seconds in an electrolyte which consisted of 20% H_2SO_4 and 80% methanol. Polishing conditions were 54°C (130°F) and 20 volts. The samples were then electrolytically etched in 10% oxalic acid at 6 volts for 10 seconds. The etching time was shorter for EBSP sample preparation (10 seconds for EBSP analysis versus 25 seconds for light microscopy) because it was necessary to have a very flat surface in order to obtain good patterns using EBSP analysis.

Kikuchi electron backscattered diffraction patterns were obtained only from grain pairs that were separated by grain boundaries which exhibited reversals of curvature. A pattern was obtained from each grain in the pair. The data from these patterns was then entered into the EBSP system software which determined the rotation angle and rotation axis between the two grains. This procedure was repeated for 90 pairs of grains that were separated by grains which exhibited reversals of curvature.

G. Transmission Electron Microscopy

Samples were evaluated on a JEOL JEM-2000FX TEM equipped with an energy dispersive x-ray spectrometer (EDS) system

operated at 200 kV. The Gleeble samples used in the present study were larger in diameter than typical Gleeble samples. A typical Gleeble sample is about 6mm (0.25 in.) in diameter. A Gleeble sample this size would yield only 1 or 2 TEM specimens. The grain size of the alloy 718 used in this study was fairly large by TEM standards and the probability that thin area would occur directly in the vicinity of a migrated grain boundary in these specimens was very low. Also, if a grain boundary was revealed during the thinning process, the grain boundary must be located perpendicular to the hole so that the concentration profiles would not be affected by the concentration gradient that arises as a function of TEM specimen thickness. If the migrated grain boundary was located perpendicular to the hole produced during thinning, concentration profiles could be obtained across a migrated grain boundary along a line where the thickness of the sample was constant.

Therefore, a 1.295cm (0.510 in.) diameter Gleeble sample was used in order to get several TEM specimens per Gleeble sample. The 1.295cm (0.510 in.) diameter sample yielded between 7 and 11 TEM specimens per Gleeble sample. This increased the probability of getting thin area in the vicinity of the migrated grain boundaries and of finding migrated grain

boundaries that were oriented perpendicular to the hole rather than parallel to the hole.

The Gleeble samples were sectioned with a diamond saw at the location of the control thermocouple and one part of the sample was prepared for analysis on the TEM. This section of the sample was marked to denote where the control thermocouple was located. The sample was sectioned again using the diamond saw in order to remove an approximately 3mm ($\frac{1}{8}$ in.) thick section of the sample which contained the area where the control thermocouple was located (See sketch in Figure 7). This 3mm ($\frac{1}{8}$ in.) thick specimen was mounted onto a 2.54cm (1in.) cylindrical steel holder using TEM mounting wax so that the specimen could be ground to a thickness of 100-150 μm (0.004-0.006 in.). The specimen was ground on 60-grit silicon carbide paper to a thickness of about 300 μm (0.012 in.) then ground on 600-grit silicon carbide paper to a final thickness of 100-150 μm (0.004-0.006 in.). Water was used as a lubricant. Disks 3 mm ($\frac{1}{8}$ in.) in diameter were cut from the sample, after grinding to 100-150 μm (0.004-0.006 in.) thickness, using a TEM sample metal punch. Approximately nine 3 mm ($\frac{1}{8}$ in.) diameter specimens were obtained from each sample.

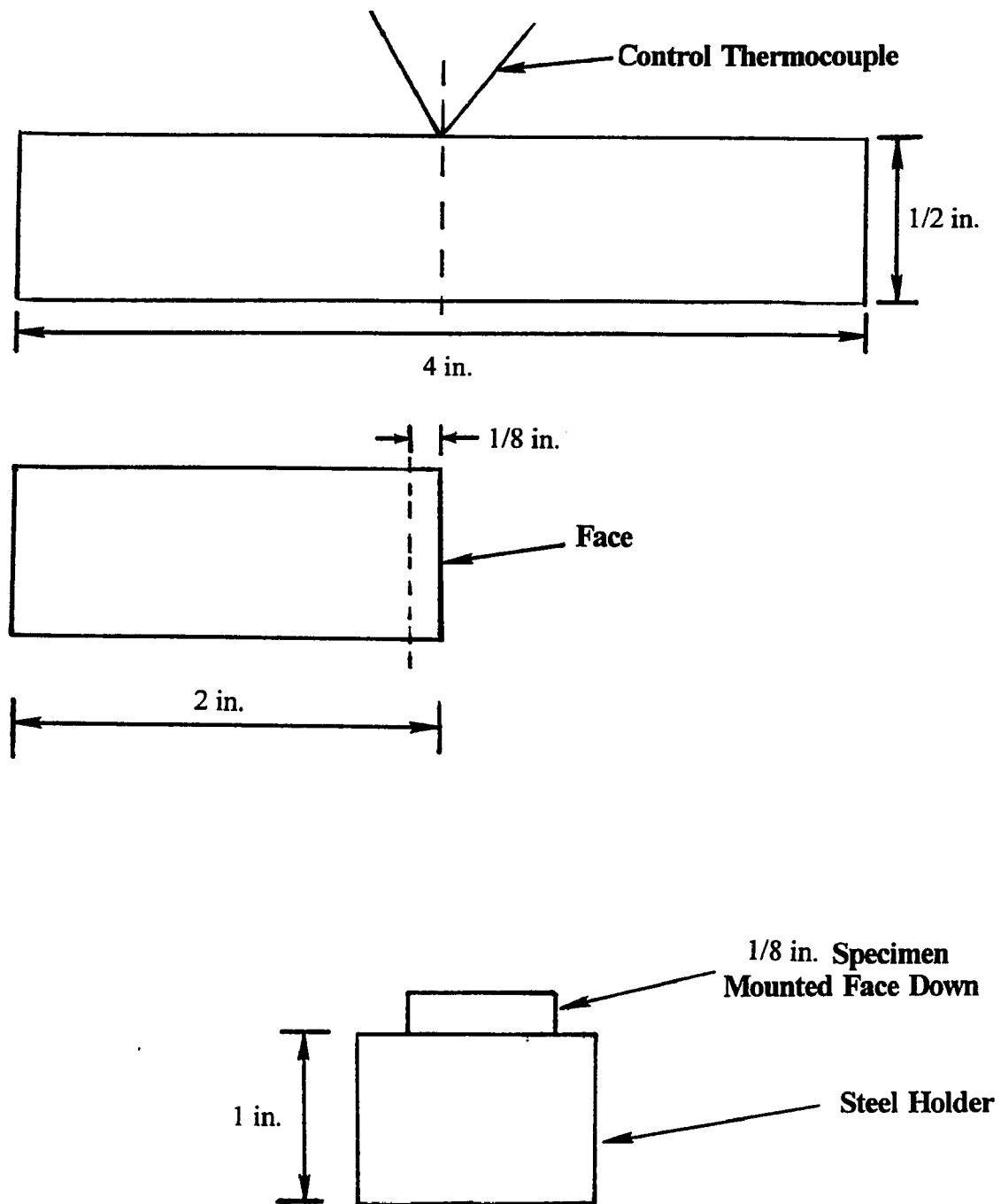


Figure 7. Sketch showing how samples were sectioned and mounted for TEM specimen preparation.

Three different electrolytes were used to determine the best one for thinning of alloy 718 using a jet polisher. The first electrolyte used consisted of 67.5% methanol, 22.5% butyl cellosolve, and 10% perchloric acid. The thinning conditions were 45 volts and -40°C . During thinning, the electrolyte became very thick and clogged the jets on the jet polisher. The specimens had to be thinned on an ion mill for about an hour after thinning on the jet polisher because this electrolyte was not effective for thinning the area located near carbides. This procedure was very time consuming and did not yield much thin area.

The second electrolyte that was tried consisted of 90% methanol and 10% perchloric acid. The butyl cellosolve was omitted because it caused the electrolyte to be very thick and clogged the jets. Preliminary results suggested that the methanol plus perchloric acid electrolyte would give better results on the jet polisher so that the ion mill would not have to be used. The best thinning conditions were determined to be 45 volts and -55°C . These conditions were based on the thinning results of as-cast alloy 718. When the same electrolyte and thinning conditions were used for the wrought alloy 718 used in the present study, the results were not as good. Although the specimens using the methanol-perchloric

acid electrolyte did have more thin area than the methanol-butyl cellosolve-perchloric acid electrolyte plus ion milling specimens, another electrolyte was tried in order to get more thin area.

The final and best electrolyte that was tried for the wrought alloy 718 that was used in this study consisted of 90% acetic acid and 10% perchloric acid. The best thinning conditions were determined to be 50 volts and 8°C. Approximately 100 TEM specimens were thinned and evaluated on the TEM in order to determine the best electrolyte and thinning conditions. About 30 of these specimens were in the as-received cast or wrought conditions. The other 70 specimens were from the 1227°C isothermal treatment samples. For the 1250°C samples, about 30 TEM specimens were examined before one was found that had thin area in the vicinity of a migrated grain boundary located perpendicular to the hole. For the 1240°C sample, about 10 TEM specimens were examined before one was found for complete TEM/EDS analysis.

TEM/EDS profiles for 1227°C, 1240°C, and 1250°C were obtained at a magnification of 10,000X using a spot size of 4L and the smallest (70 μm diameter) platinum top hat condenser aperture. The distance between adjacent data point along the EDS profile data line was approximately 1 μm for the 1240°C

and 1250°C specimens and approximately 0.5 μm for the 1227°C specimen. From the TEM analysis, the niobium concentration in the migrated regions relative to that in the matrix was determined. There were no standards used in the TEM/EDS analysis for determining the semi-quantitative values of the niobium concentration. The relative differences between the niobium concentrations in the matrix and the migrated region were determined, not the actual quantitative values.

H. Auger Electron Microscopy

Sample preparation for analysis on an Auger electron microscope consisted of grinding from 240 grit through 600 grit silicon carbide followed by polishing with 6, 3, and 1 micron diamond paste. Samples were then etched in 10% oxalic acid at 6 volts for 25-30 seconds. The samples were sputtered to minimize the oxygen peak. Spectra were collected over a range of 0 eV to 2000 eV using a beam size of 1 μm at 10 kV and 3×10^{-7} A. Auger analysis was used in order to detect any changes in concentration of light elements such as carbon, boron, and nitrogen that are not detectable using TEM/EDS analysis.

RESULTS

A. As-Received Condition

The microstructure of alloy 718 in the as-received condition is shown in Figure 8. The microstructure consisted of carbides and Ni_3Nb (δ phase) in a γ matrix. This is consistent with the microstructure for wrought alloy 718 in the as-received condition as was shown by previous researchers (30).

B. As-Heat Treated Condition

The as-heat treated alloy 718 was investigated using light microscopy. The microstructure consisted of large grains (γ matrix) with intergranular and intragranular niobium carbide particles. Heat treatment at 650°C for 4 hours promoted trapping of some niobium carbide particles on the grain boundaries. Figure 9 shows the microstructure of alloy 718 after the 650°C for 4 hours heat treatment. The arrows point to niobium carbide particles on the grain boundaries.

C. 1227°C Isothermal Treatment

The 1227°C samples, that were produced by rapid thermal cycle in the Gleeble, were investigated using light

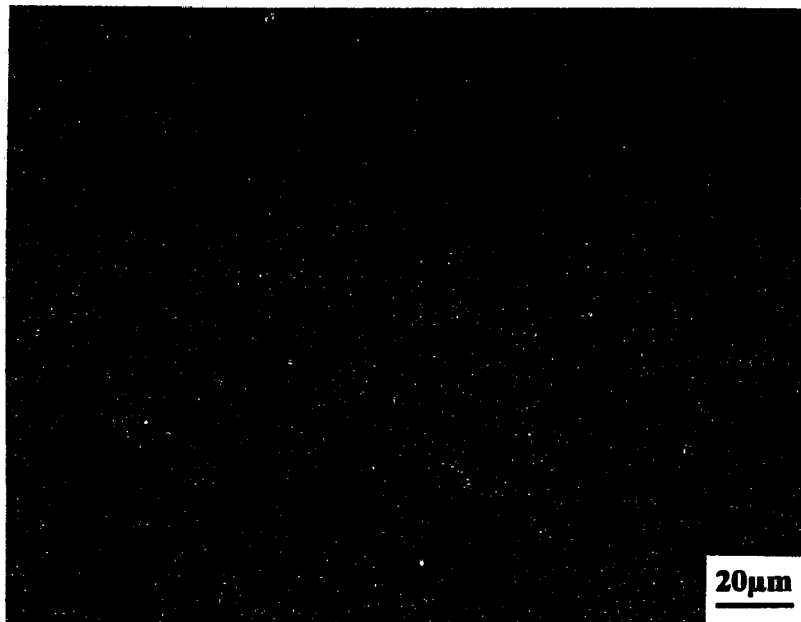


Figure 8. Light micrograph of as-received condition of alloy 718. Microstructure consists of carbides and Ni_3Nb (δ phase) in the γ matrix.

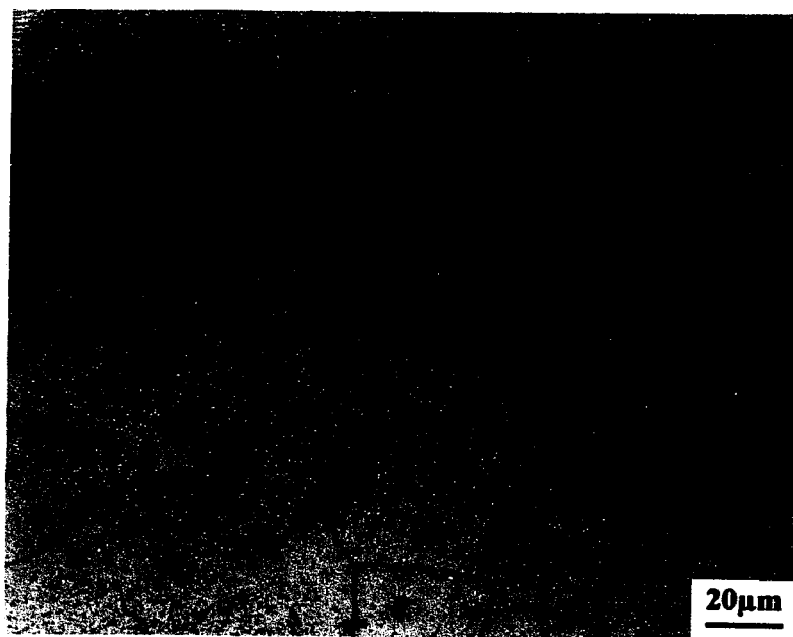


Figure 9. Light microscope image showing the microstructure of alloy 718 after the 650°C for 4 hours heat treatment. The arrows point to niobium carbides on the grain boundaries.

microscopy, SEM, TEM, and EBSP techniques. The microstructure of alloy 718 after isothermal treatment of 1227°C for 4 seconds is shown in Figure 10a (light micrograph) and Figure 10b (SEM SE image). The original position of the grain boundary is denoted by OGB and the position of the grain boundary after migration is denoted by CLFM. These micrographs show that the migrated boundary has reversed curvature. That is, the migrated grain boundary zigzags back and forth across the original grain boundary position.

The TEM bright-field image of the 1227°C for 4 seconds sample is shown in Figure 11. This micrograph shows the areas where TEM/EDS profiles were obtained. Representative TEM/EDS spectra from the matrix and the migrated region (area behind the migrated boundary) are shown in Figure 12. These spectra show that the concentration of niobium in the migrated region was higher than the niobium concentration in the matrix. A plot of the niobium concentration as a function of distance is shown in Figure 13. The average Nb concentration in weight percent was 9.3% (range 7.6-10.6) for the migrated region and 5.9% (range 5.7-6.4) for the matrix.

A total of 90 pairs of grains separated by migrated boundaries after CLFM were randomly chosen for EBSP analysis. All of the grains that were evaluated on the EBSP system for

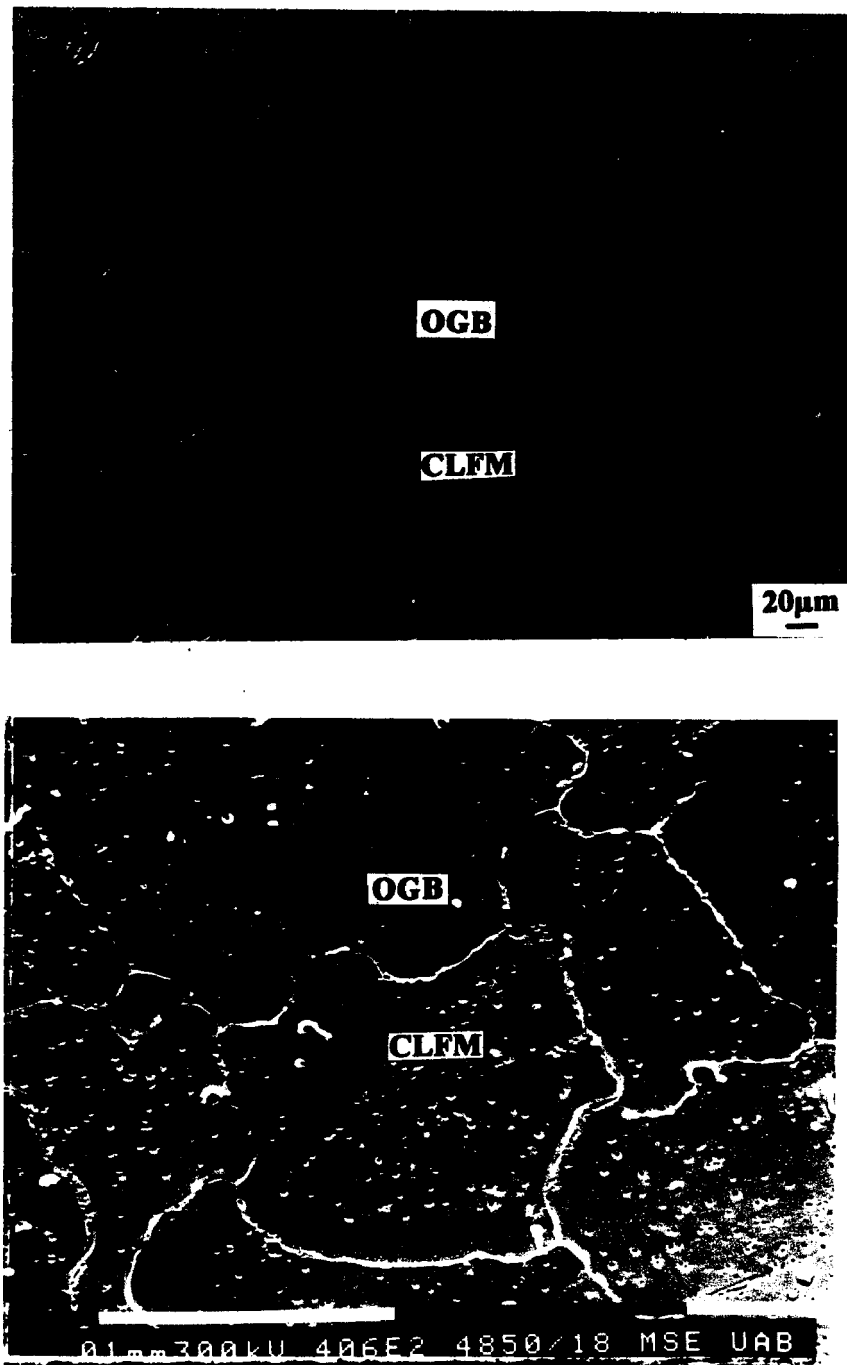


Figure 10. (a) Light micrograph and (b) SEM micrograph of 1227°C peak temperature sample showing the original grain boundary position (OGB) and a grain boundary with reversed curvature as a result of CLFM (CLFM).

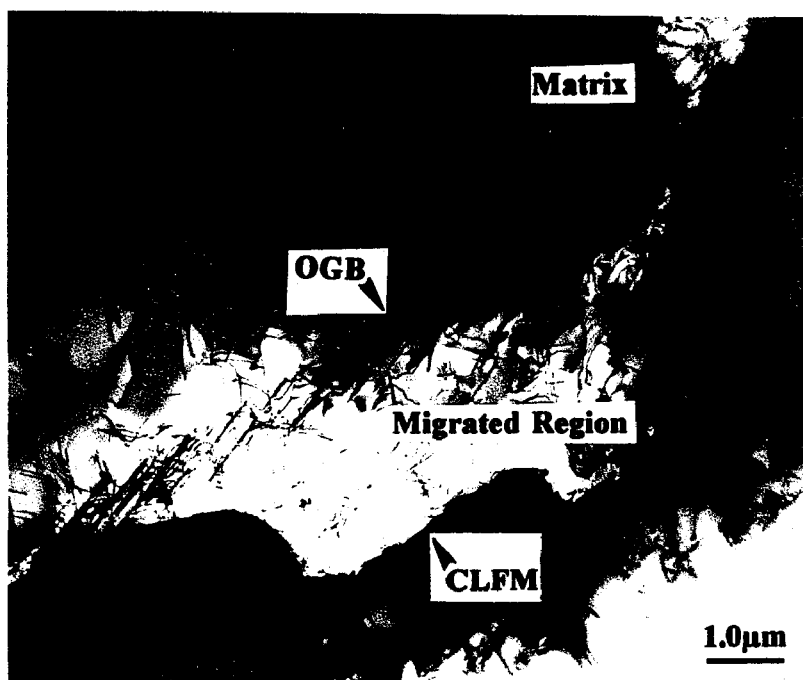


Figure 11. TEM bright-field image of 1227°C peak temperature sample showing area where TEM/EDS profiles were obtained.

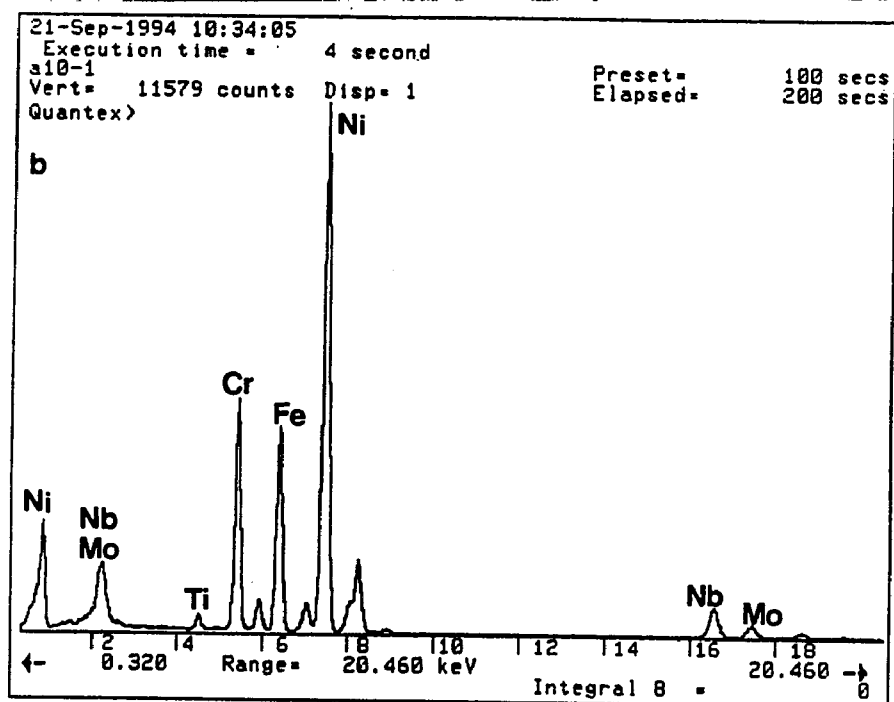
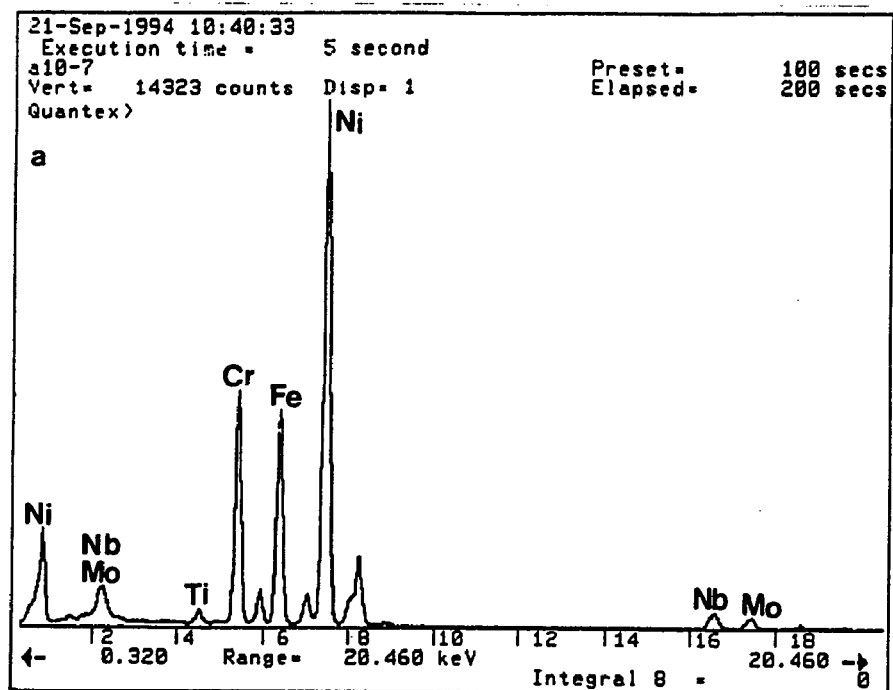


Figure 12. Representative TEM/EDS spectra from the a) matrix and b) migrated region of the 1227°C peak temperature sample.

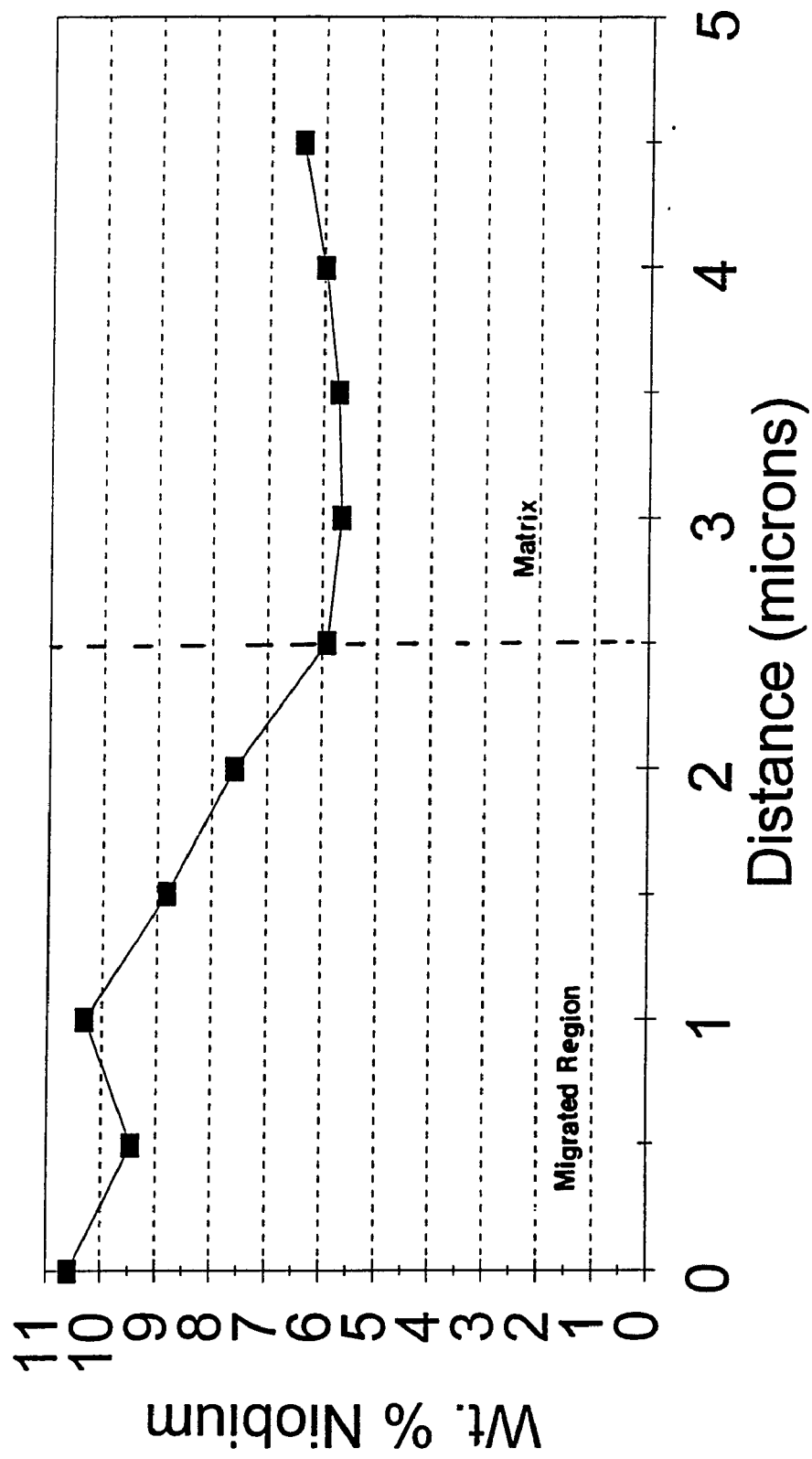


Figure 13. Niobium concentration versus distance profile for the 1227°C sample.

the crystal orientation determination were separated by boundaries with reversed curvatures like that shown in Figure 14 (Figure 14 is representative of typical areas where orientation analysis was performed). Representative EBSP patterns taken from two alloy 718 grains that were separated by a CLFM grain boundary are shown in Figure 15. The crystal orientations determined from EBSP analysis are given in Table V and were characterized as follows: low angle boundaries (<15 deg), close to low angle boundaries (15-20 deg), high angle boundaries (>20 deg), and CSL ($v/u_m < 1$, where v is the angular deviation from exact CSL and u_m is the maximum allowable deviation from exact CSL (34)). One of the migrated boundaries was a low angle boundary, 3 were close to low angle boundaries, 84 were high angle boundaries, and 2 were CSLs (29).

D. 1240°C Isothermal Treatment

The 1240°C for 4 seconds isothermal treatment was investigated using light microscopy, SEM, and TEM techniques. The light micrograph for this condition is shown in Figure 16. The original grain boundary position and migrated grain boundary are denoted by arrows in Figure 16. The migrated grain boundary for this condition also exhibits reversal of curvature.

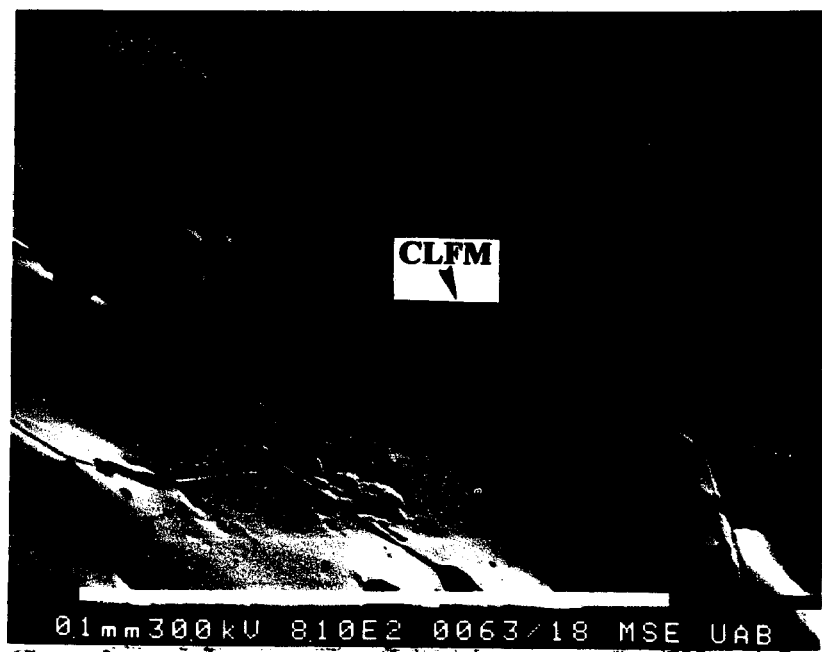


Figure 14. Representative SEM micrograph of typical areas where orientation analysis was performed for the 1227°C peak temperature sample. The migrated grain boundary is denoted by CLFM. The image was taken using the approximately 70° tilt necessary for EBSD analysis.

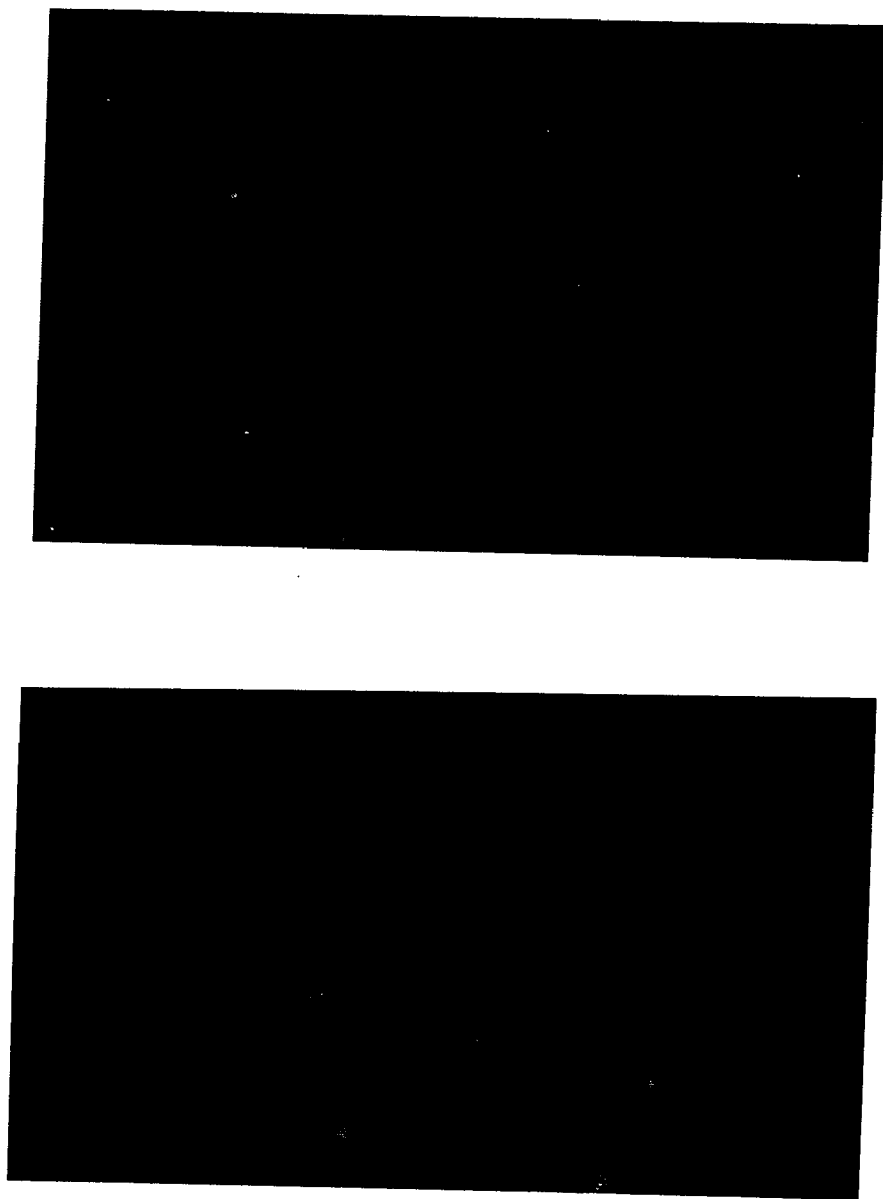


Figure 15. EBSD patterns from two alloy 718 grains that were separated by a CLFM grain boundary.

Table V. Characterization of Migrated Grain Boundaries

Low Angle (<15 deg)	Close to Low Angle (15-20 deg)	High Angle (>20 deg)	CSL ($u/u_m < 1$)
1	3	84	2

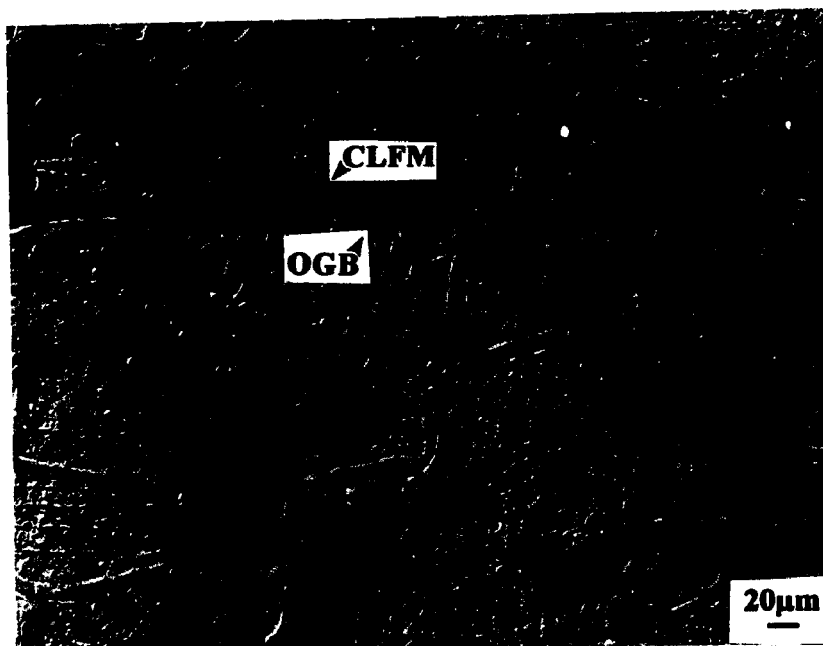


Figure 16. Light micrograph of 1240°C peak temperature sample showing the original grain boundary position (OGB) and a grain boundary with reversed curvature as a result of CLFM (CLFM).

The area where TEM/EDS analysis was performed is shown in the TEM bright-field image in Figure 17a. Figure 18 shows representative TEM/EDS spectra from the matrix and the migrated region. The plots for niobium concentration as a function of distance are shown in Figures 19, 20, and 21. Figures 19, 20, and 21 were collected along points on data line 1, 2, and 3, respectively, that are shown in Figure 17a. Since the original grain boundary positions cannot be seen in the TEM bright-field image, an SEM secondary electron image (Figure 17b) is shown which has an area (boxed region) that is similar to the region shown in the TEM bright-field image in Figure 17a. In Figure 17b, the original grain boundary positions and the migrated regions can be clearly distinguished. This also suggests where the original grain boundary positions and migrated regions are located in the TEM bright-field image. Data lines are drawn in Figure 17b to show how the data lines in Figure 17a can go through more than one migrated region, which can be used to explain the appearance of the niobium concentration versus distance plots for the 1240°C sample.

Observe data line 1 drawn in Figure 17b. This data line goes through a migrated region that is located to the left of the migrated grain boundary. The concentration of niobium in

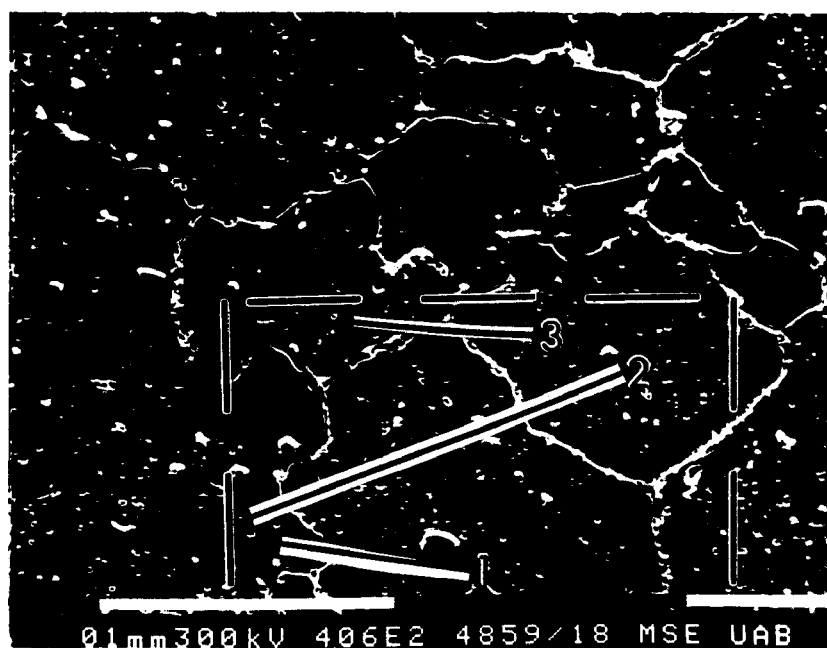
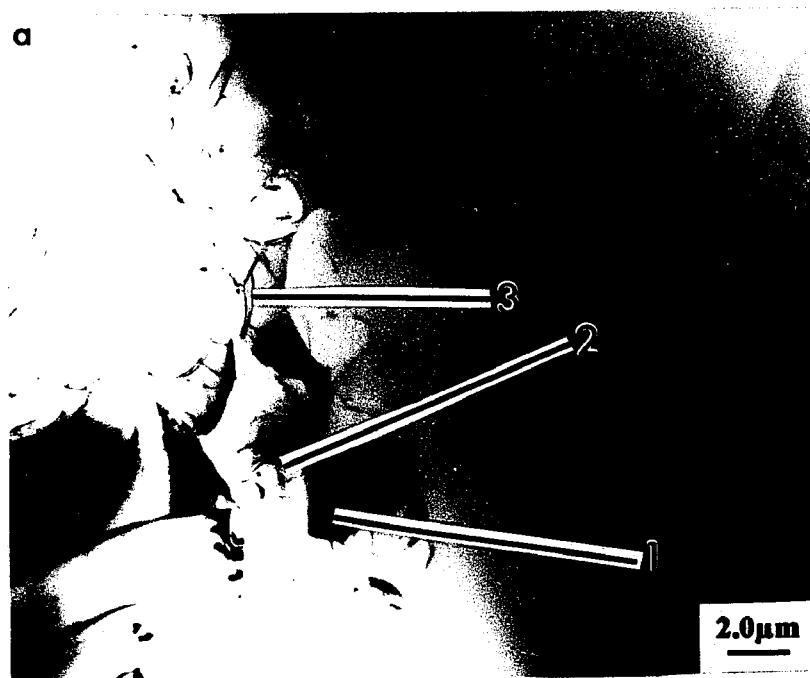


Figure 17. (a) TEM bright-field image showing area where TEM/EDS profiles were obtained for the 1240°C peak temperature sample. (b) SEM secondary electron image of an area (boxed region) that is similar to the TEM image shown in (a).

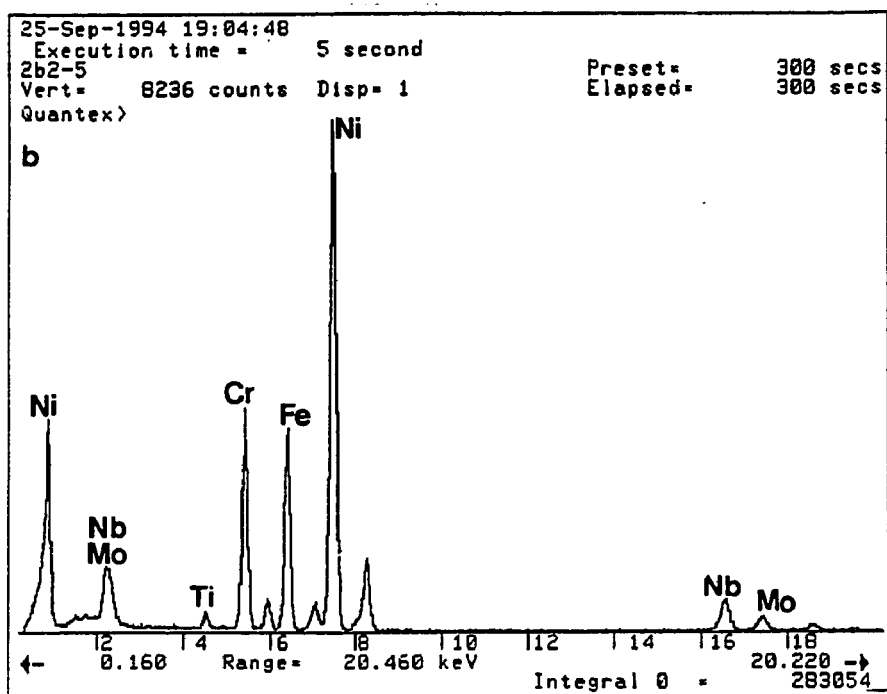
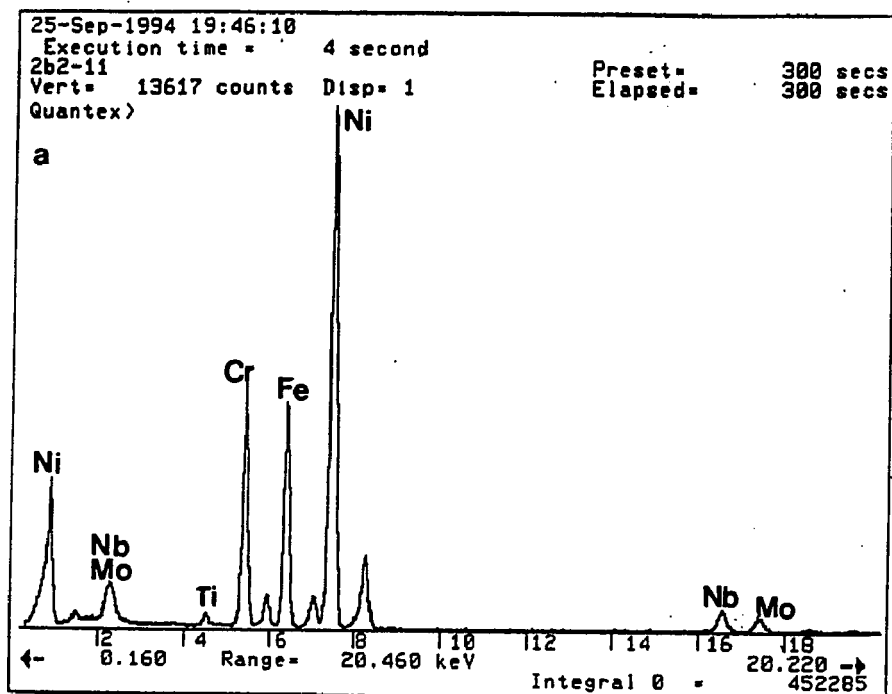


Figure 18. Representative TEM/EDS spectra from the a) matrix and b) migrated region of the 1240°C peak temperature sample.

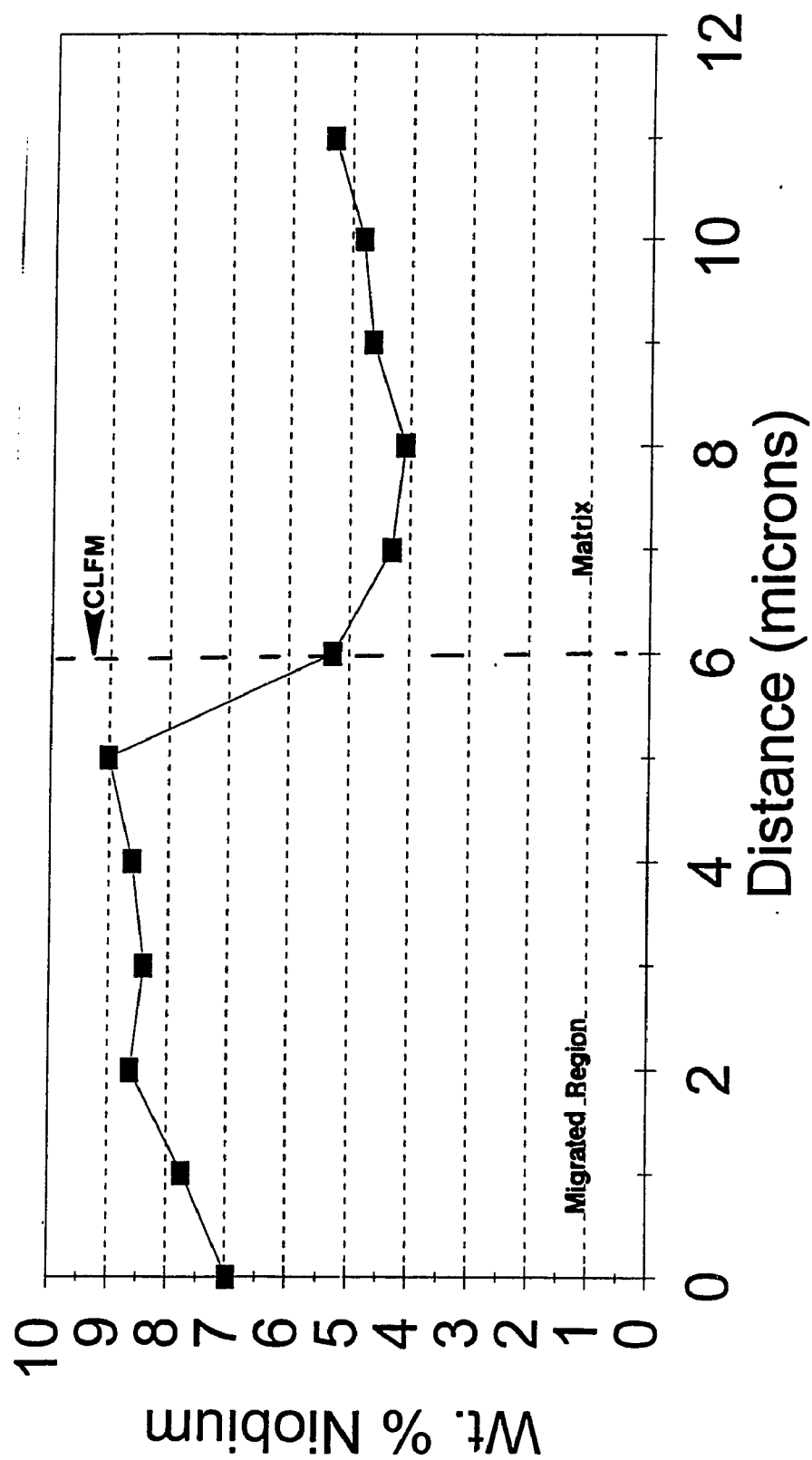


Figure 19. Niobium concentration versus distance profile for 1240°C collected along data line 1 shown in Figure 17a.

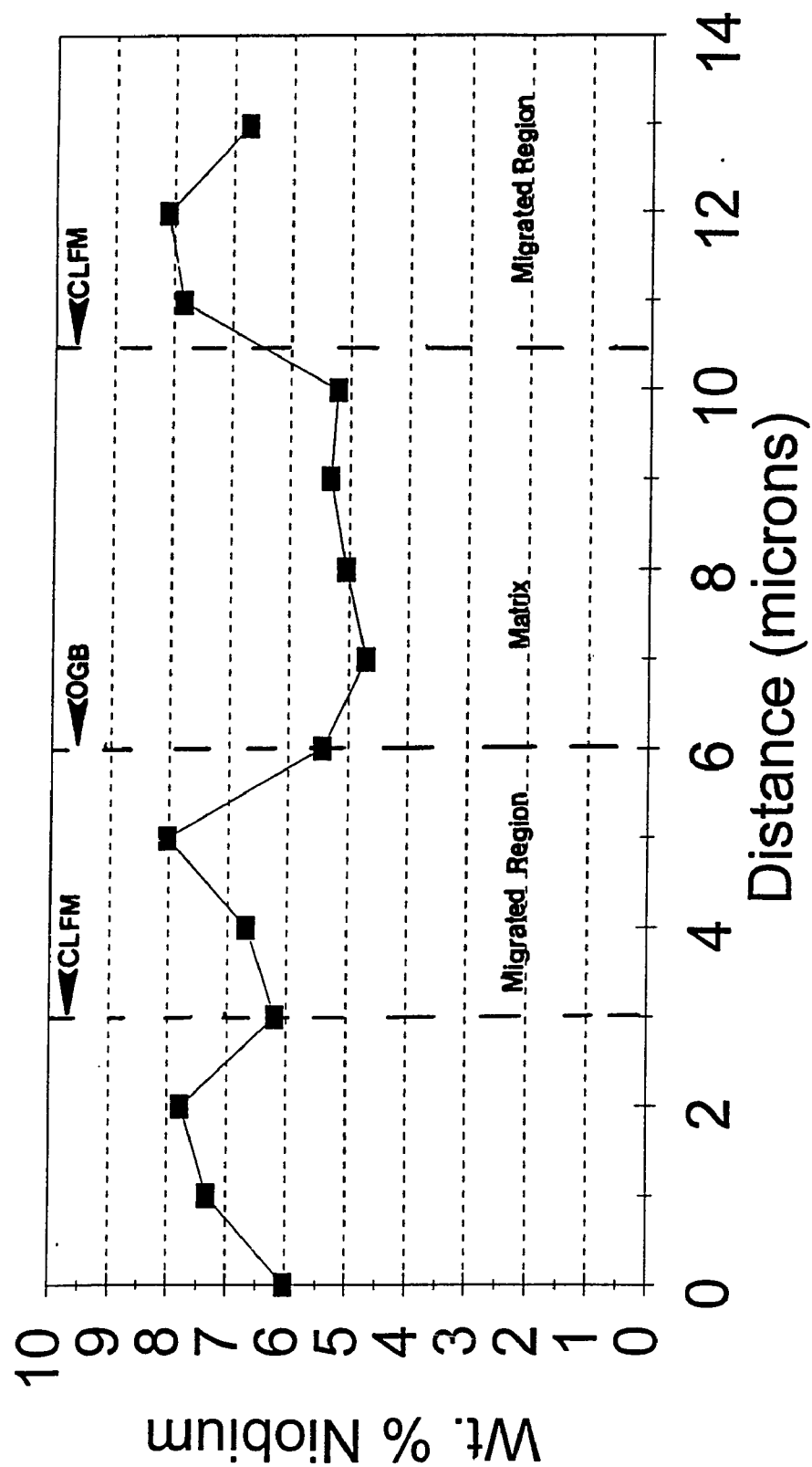


Figure 20. Niobium concentration versus distance profile for 1240°C collected along data line 2 shown in Figure 17a.

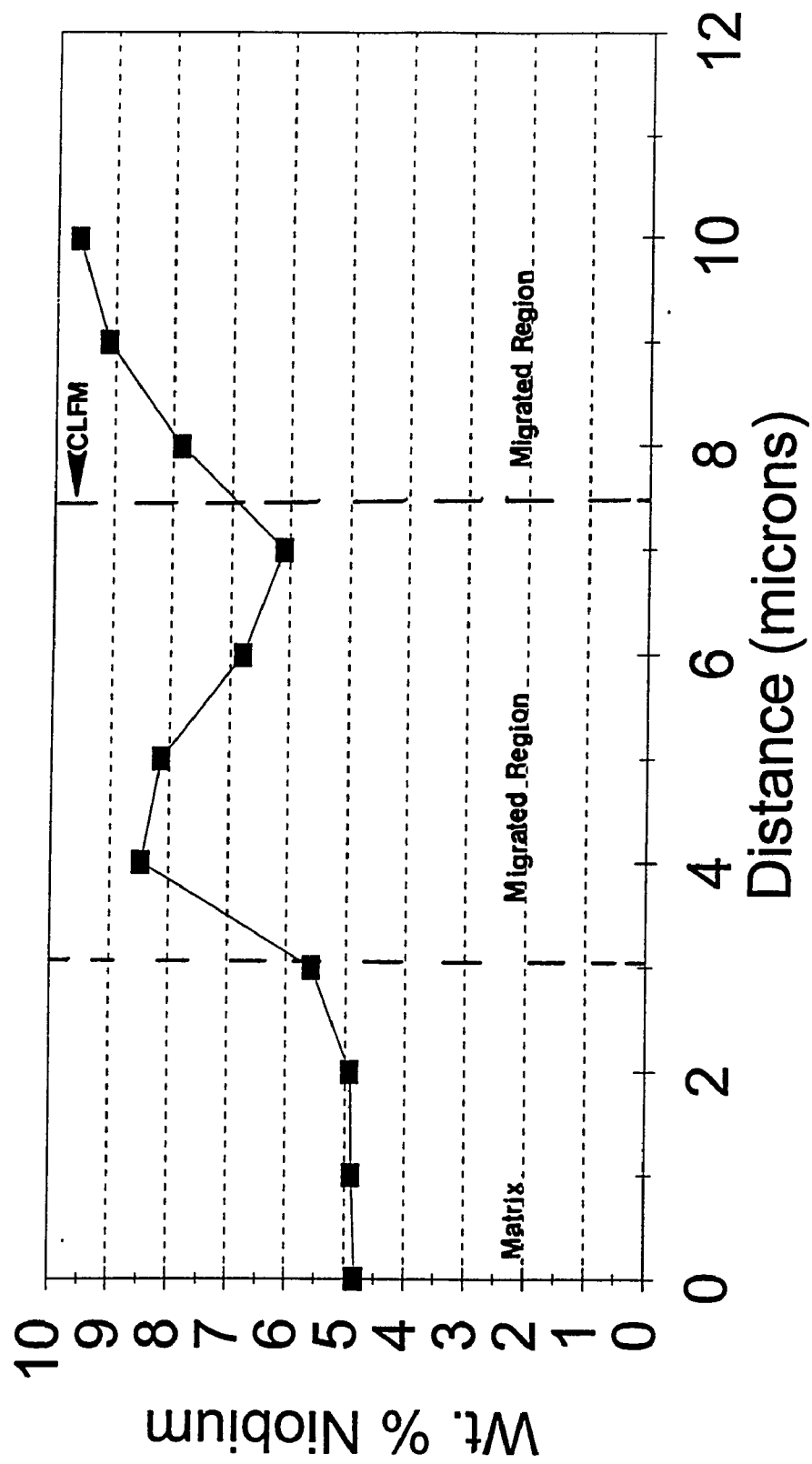


Figure 21. Niobium concentration versus distance profile for 1240°C collected along data line 3 shown in Figure 17a.

this region is denoted on the plot in Figure 19 by points 0 through 5 on the x-axis. At point 6 on the x-axis, the data line now goes through the matrix located to the right of the migrated grain boundary. This shows how data line 1 drawn in the SEM micrograph explains the niobium concentration versus distance plot obtained from the EDS profile obtained along data line 1 drawn in the TEM micrograph in Figure 17a.

The appearance of the niobium concentration versus distance plot for data line 2 (Figure 20) shown in the TEM micrograph in Figure 17a suggests that the EDS profile obtained along data line 2 went through a migrated region, the matrix, then through another migrated region. This was assumed since the niobium concentration was relatively high from points 0 through 5 and then decreased between points 6 and 10. The niobium concentration increased again between points 11 and 13. In other words, as shown in Figure 20, the highest niobium concentration occurred in the migrated regions that were located between the original grain boundary position and the migrated grain boundary. Data line 2 drawn in the SEM micrograph in Figure 17b shows how the EDS profile obtained along data line 2 shown in the TEM micrograph could have gone through two migrated regions.

Observe the left side edge of data line 2 in Figure 17b. The migrated region is located to the right of the grain boundary (migrated grain boundary) that is located near the left-hand edge of data line 2. The data line then goes through the interior of the grain which consists of the matrix. This is the area which lies between data points 6 and 10 on the plot in Figure 20. Data line 2 then hits another grain boundary (migrated grain boundary) located near the right edge of data line 2 in Figure 17b. To the right of this second grain boundary is another migrated region. This shows how the EDS profile obtained along data line 2 in the TEM micrograph in Figure 17a could have gone through a migrated region, the matrix, then another migrated region that would have resulted in the niobium concentration being high, low, then high again as shown in the niobium concentration versus distance plot in Figure 20.

The niobium concentration versus distance plot obtained along data line 3 in Figure 17a is shown in Figure 21. Figure 21 shows that data line 3 went through the matrix and then through two migrated regions located adjacent to each other. Data line 3 in Figure 17a must have gone through an area like that shown at the top of the boxed region in Figure 17b. Going from left to right, data line 3 in Figure 17b is shown to go

through the matrix before it hits a migrated grain boundary that has a migrated region located below it. The data line then hits another migrated grain boundary and goes through another migrated region located to the right of the second migrated grain boundary.

Data line 3 drawn in the SEM micrograph in Figure 17b is shown to go through the matrix then through two different migrated regions located adjacent to each other. Therefore, this shows how data line 3 in Figure 17b explains how the EDS profile obtained along data line 3 shown in Figure 17a results in the plot shown in Figure 21. This is because the TEM/EDS profile along data line 3 must have gone through the matrix and two adjacent migrated regions like that shown in the SEM micrograph in Figure 17b. Overall, the average niobium concentration was determined to be 7.8% (range 6.0-9.6) in the migrated region and 5.0% (range 4.1-5.6) in the matrix.

E. 1250°C Isothermal Treatment

The 1250°C for 4 seconds isothermal treatment was examined using light microscopy, SEM, and TEM methods. The light micrograph for this condition is shown in Figure 22a. The original grain boundary position was defined as the area that separated the clear, clean region from the region that contained particles which gave the region a mottled

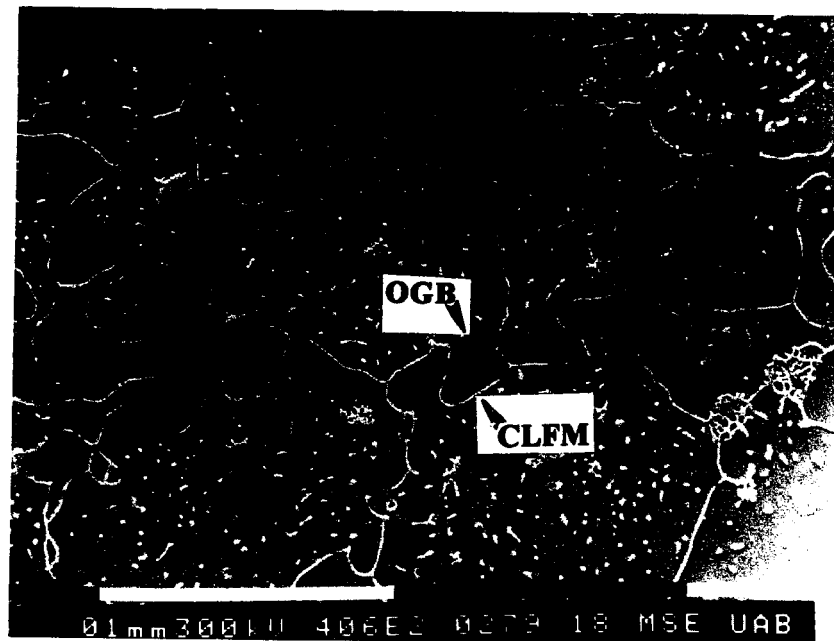
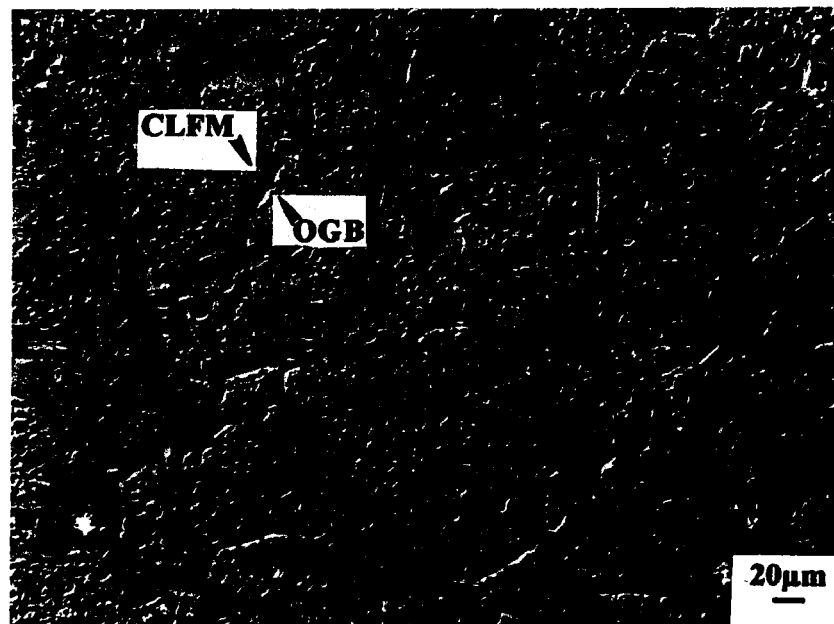


Figure 22. (a) Light micrograph and (b) SEM micrograph of 1250°C peak temperature sample showing the original grain boundary position (OGB) and a grain boundary with reversed curvature as a result of CLFM (CLFM).

appearance. The clear regions are the areas that were swept by the migrated boundary. Figure 22b is a representative SEM micrograph for the 1250°C for 4 seconds sample. This micrograph clearly shows that the migrated regions (areas swept by moving boundaries) are different in appearance from the matrix. This contrast, which occurs between the migrated region and the matrix, has been attributed to the etchant being sensitive to the occurrence of a composition change in the newly formed solid region located near the migrated grain boundary (6,7,16,17,23,25).

The area where TEM/EDS analysis was performed is shown in the TEM bright-field image in Figure 23. Figure 24 shows representative TEM/EDS spectra from the matrix and the migrated region. The niobium concentration across the migrated region and the matrix is shown in Figure 25 as a plot of niobium concentration versus distance. Observation of this plot shows that the niobium concentration appears to decrease slightly upon approaching the migrated grain boundary (denoted as liquid film). Once across the migrated grain boundary, the niobium concentration starts off slightly low then it increases to an approximately uniform value in the matrix. The average niobium concentration was determined to be 4.2% (range 3.5-5.0) in the migrated region and 4.0% (range 3.6-4.6) in

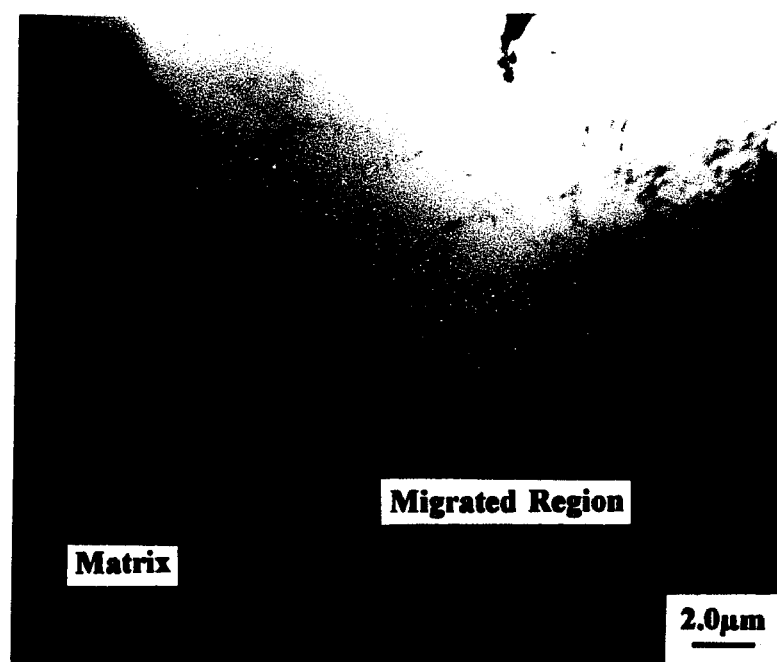


Figure 23. TEM bright-field image showing area where TEM/EDS profiles were obtained for the 1250°C peak temperature sample.

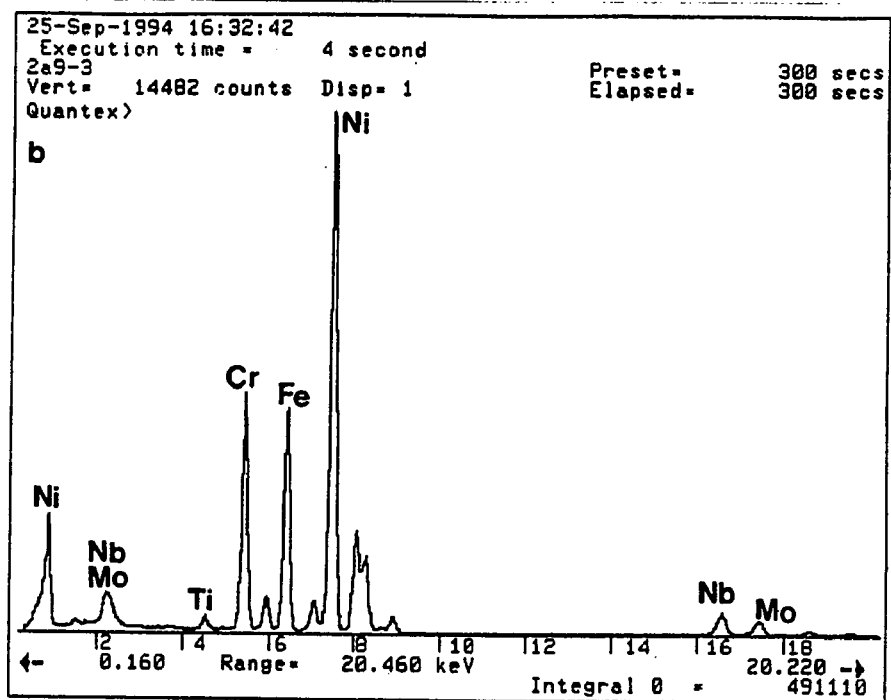
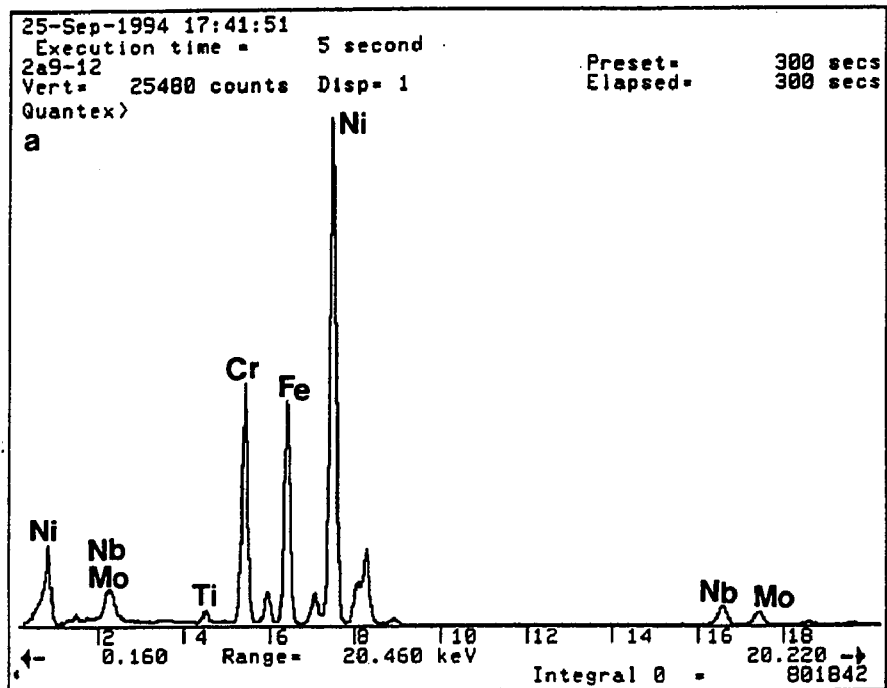


Figure 24. Representative TEM/EDS spectra from the a) matrix and b) migrated region of the 1250°C peak temperature sample.

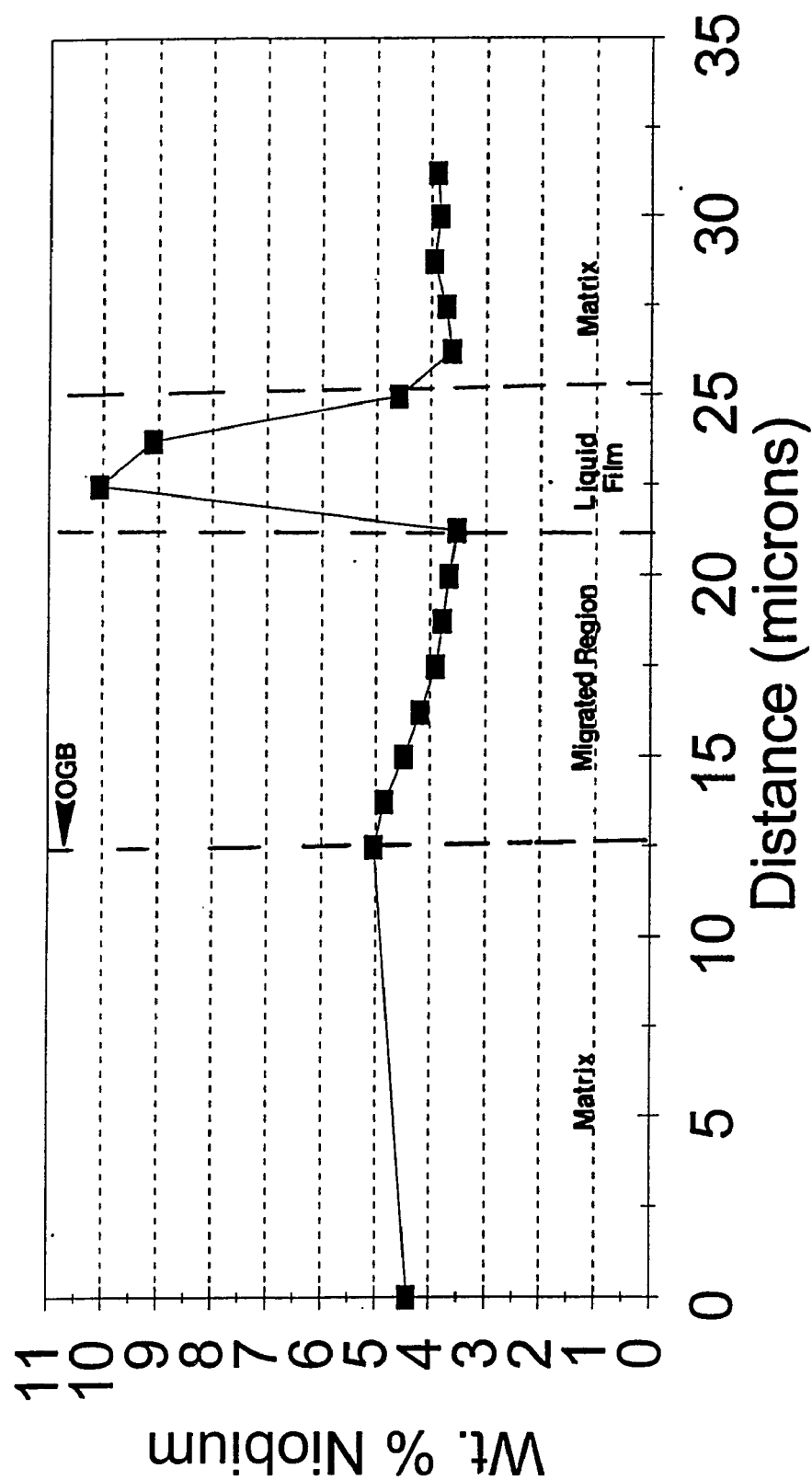


Figure 25. Niobium concentration versus distance profile for 1250°C.

the matrix. Although the niobium concentrations in the migrated region and the matrix were relatively close, there was still enough of a composition change between the matrix and the migrated regions to result in an etching contrast between the two regions.

F. 1260°C Isothermal Treatment

The 1260°C for 4 seconds isothermal treatment specimen was investigated using light microscopy and the SEM. As shown in Figure 26, the original grain boundary position is indistinguishable from the matrix. This made it difficult to determine whether the grain boundaries were actually CLFM boundaries. Therefore, TEM analysis was not performed for the 1260°C for 4 seconds isothermal treatment.

G. Auger Electron Analysis

Auger analysis was performed on the 1227°C and 1240°C samples to see if segregation or depletion of carbon, boron, or nitrogen occurred in the migrated regions of these samples where niobium segregation was observed. Carbon and boron could not be detected using TEM/EDS analysis. Representative Auger spectra for a migrated region and the matrix from the 1227°C sample are shown in Figures 27 and 28, respectively. The Auger spectra for the 1240°C sample was similar to those shown for 1227°C. Auger analysis showed no carbon, boron, or nitrogen

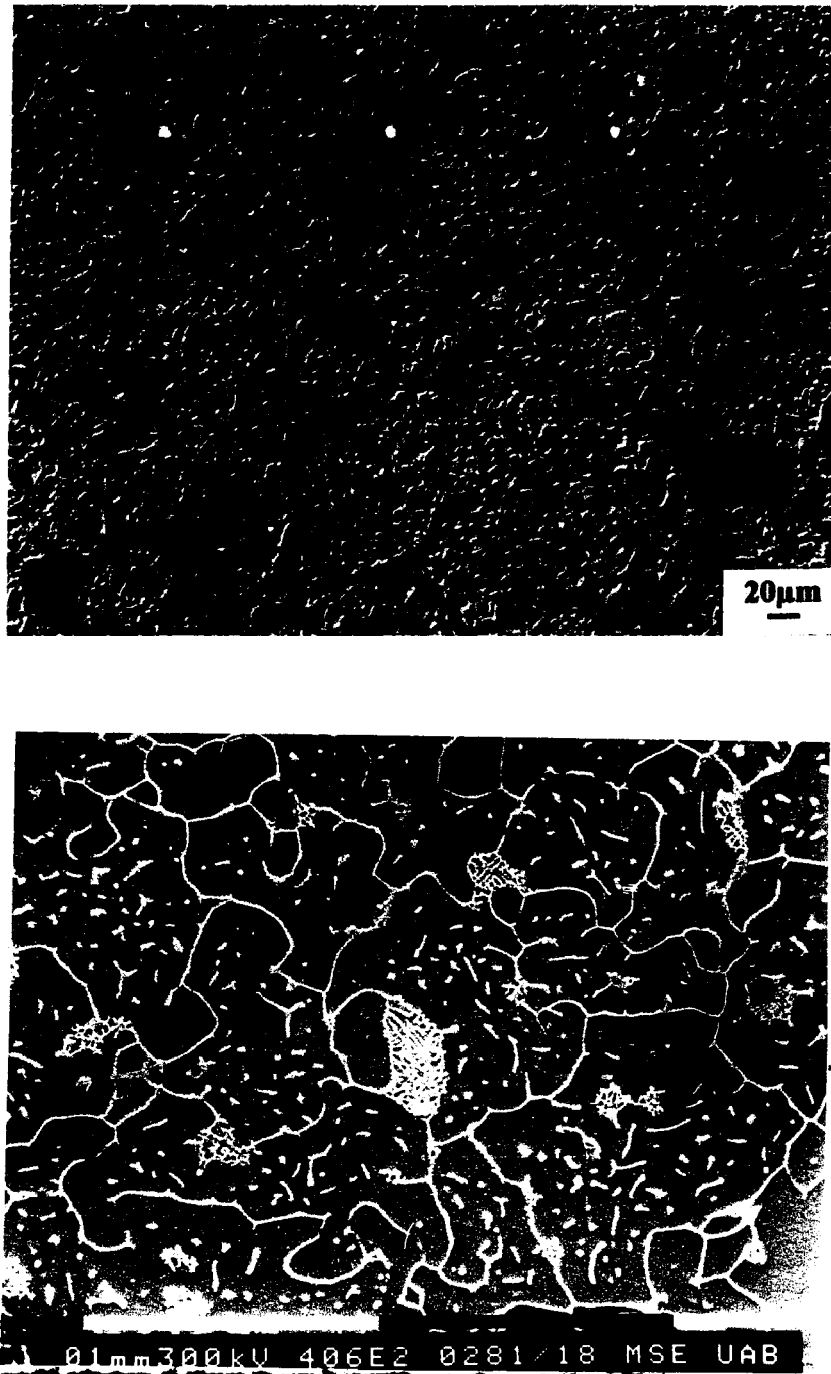


Figure 26. (a) Light micrograph and (b) SEM secondary electron image of alloy 718 for the 1260°C peak temperature sample.

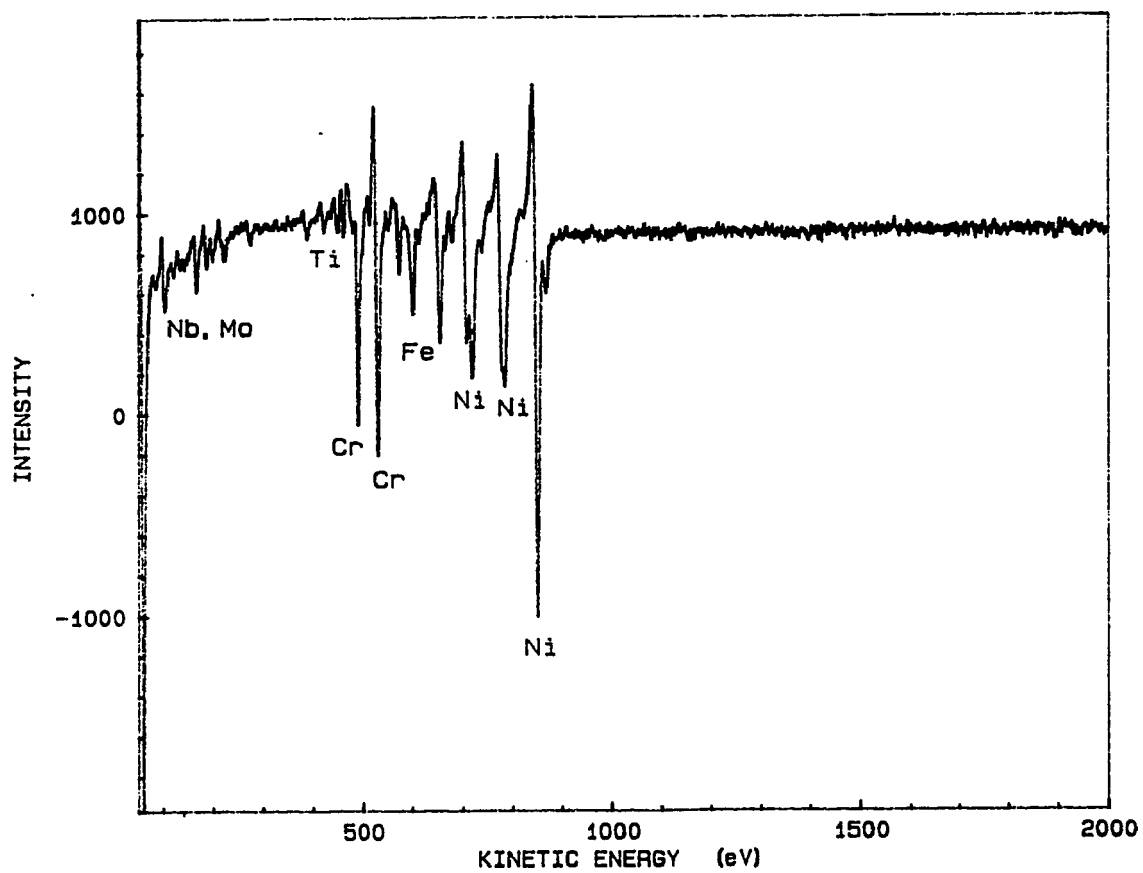


Figure 27. Auger spectrum from the migrated region of the 1227°C sample.

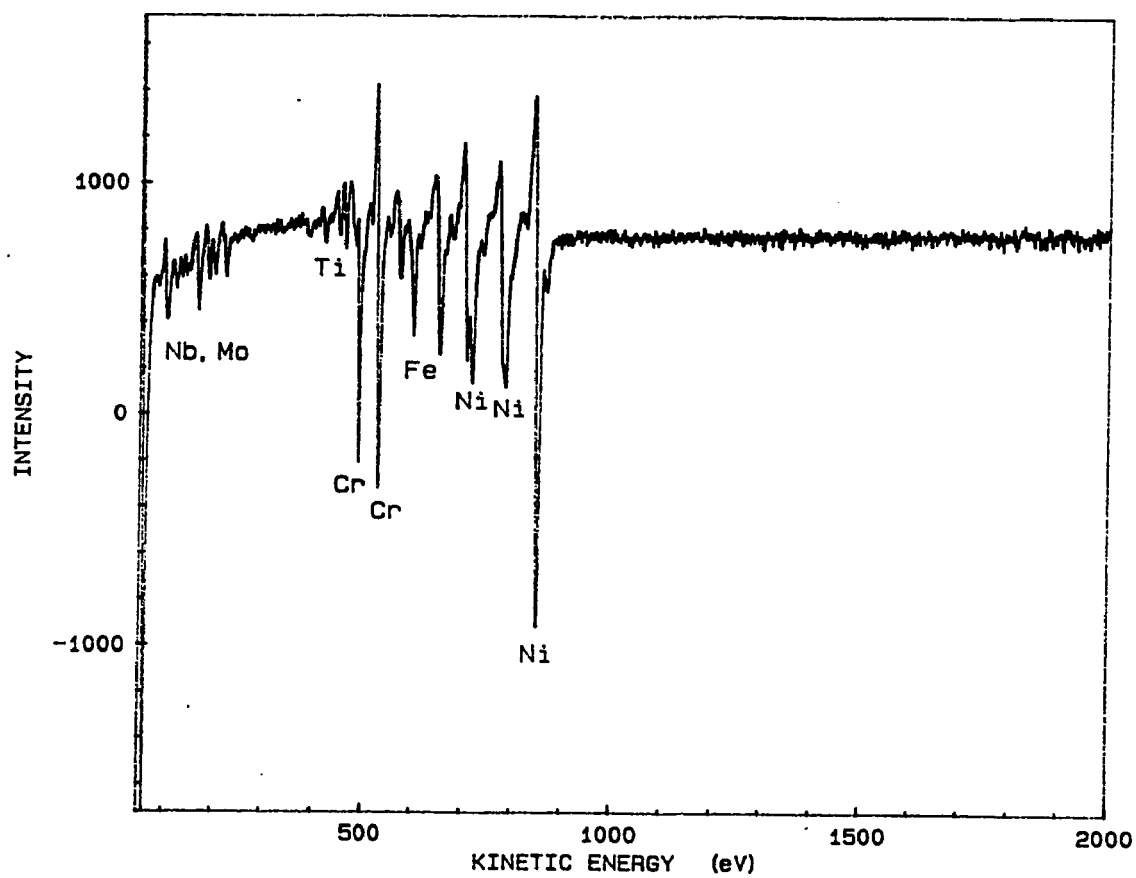


Figure 28. Auger spectrum from matrix of the 1227°C sample.

segregation in the migrated regions. There was also no depletion of these elements in this region.

H. Migration Rates

The migration rates were determined by measuring the maximum migration distance and dividing it by the time held at the peak temperature. All of the migrated boundaries that were chosen for measurement exhibited the characteristics of CLFM boundaries. The average migration distances and the migration rates are shown in Table VI. A plot of migration rates as a function of temperature is shown in Figure 29.

I. Niobium Diffusivity

Radhakrishnan and Thompson (27) reported the diffusivity of niobium in the matrix to be

$$D = 300 \times \exp \left(\frac{-35,800}{T} \right) \frac{\text{cm}^2}{\text{sec}}$$

The diffusivity of niobium in the matrix was calculated for 1227°C, 1240°C, 1250°C, and 1260°C for the present study and are shown in Table VII.

Table VI. Average Migration Distances and Migration Rates

Temperature (°C)	$\overline{1/\sigma_A}$ (1/ μm)	σ_T (μm)	Migration Rate ($\mu m/sec$)
1227	0.098	6.531	1.633
1240	0.090	7.111	1.778
1250	0.089	7.191	1.798

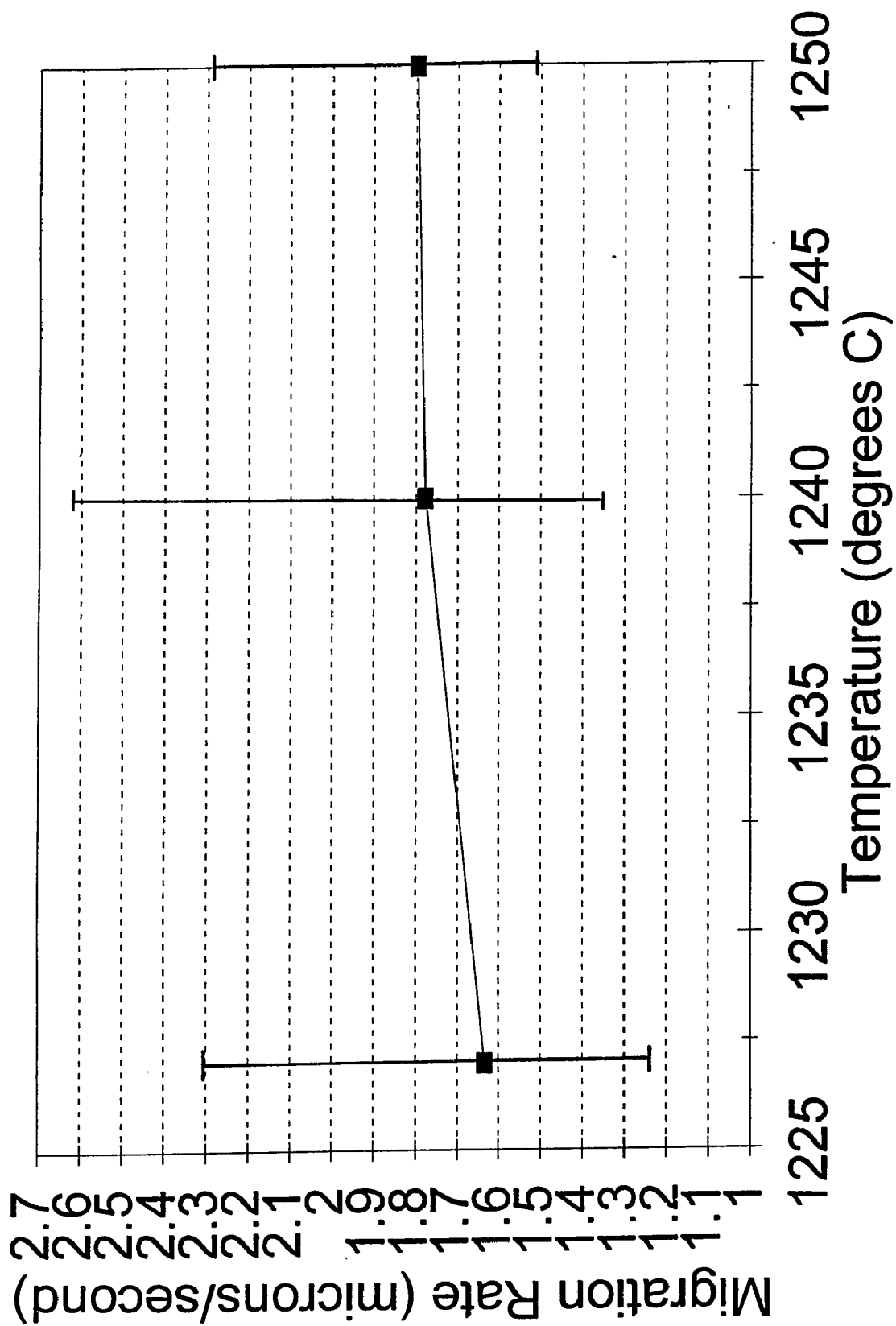


Figure 29. Migration rate plotted as a function of temperature.

Table VII. Diffusivity of Niobium in the Matrix

Temperature (°C)	Diffusivity (cm ² /sec)
1227	1.294×10^{-8}
1240	1.589×10^{-8}
1250	1.856×10^{-8}
1260	2.163×10^{-8}

DISCUSSION

A. Confirmation of Constitutional Liquid Film Migration

1. Movement Away from Center of Curvature:

The rapid thermal cycles produced in the Gleeble did promote CLFM in the alloy of this study for peak temperatures of 1227°C, 1240°C, and 1250°C. CLFM was confirmed by the fact that the grain boundaries moved away from their centers of curvature. The migration away from curvature means that there must be a driving force which overcomes the curvature driven migration normally observed.

2. Formation of a New Solid Solution:

Another feature that confirmed CLFM was the formation of a new solid solution behind the migrated grain boundary. The formation of a new solid solution was evident from the observation that the migrated regions etched differently from the matrix. Previous researchers (6,7,16,17,23,25) have attributed this contrast, which occurs between the migrated region and the matrix, to the sensitivity of the etchant to a composition change in the newly formed solid region located behind the migrated grain boundary.

3. Reversal of Curvature:

CLFM was also confirmed by the reversals of curvature of the migrated grain boundaries that are shown in Figures 10, 16 and 22. This reversal of curvature of the grain boundaries is a characteristic of CLFM and has been shown to be due to both uniform and nonuniform stress relaxation mechanisms (9). When the coherency strain becomes larger than the energy required to create dislocations in the matrix, stress relaxation occurs uniformly by plastic deformation in the matrix. This leads to a loss of coherency in the grain (9).

Whenever a loss of coherency occurs, the migration direction reverses since there is no longer a driving force for migration in the same direction. In this case, the grain boundary initially migrates in the direction of the grain with the higher orientation dependent modulus. When a loss of coherency occurs in this grain, the grain boundary migration direction gets reversed and the boundary moves in the opposite direction. In some instances, after reversal, the grain boundary moved into the other grain after passing through the original grain boundary position (35).

A loss of coherency can also occur due to a nonuniform stress relaxation across the grain boundary. The stresses due to coherency strain can relax nonuniformly by the interaction

of the stress field with the existing dislocations in the matrix. If nonuniform stress relaxation occurs, migration would begin at each site of stress relaxation (9). This leads to the local bowing of the grain boundary. That is, in this case, the migrated grain boundary appears to zigzag back and forth across the original grain boundary position. This was observed in the present study for 1227°C (Figure 10), 1240°C (Figure 16), and 1250°C (Figure 22).

In the TEM image for the 1227°C sample (Figure 11), it was observed that a wall of dislocations was left at the original position of the grain boundary. Handwerker (9) stated that this wall of dislocations at the original grain boundary position occurred when the change in lattice parameter with composition is large. A wall of dislocations at the original grain boundary position was also observed by other researchers (3, 36). However, no wall of dislocations is observed at the original grain boundary position when the change in lattice parameter with composition is small. In this situation, the strain due to the change in lattice parameter with composition is accommodated elastically and thus, no wall of dislocations is observed at the original grain boundary position (9). This is believed to be the case for the present study since the TEM images for 1240°C (Figure 17) and 1250°C (Figure 23) showed

that there were no walls of dislocations observed at the original grain boundary positions.

4. Difficulty in Confirming CLFM:

The original grain boundary position is indistinguishable from the matrix in the 1260°C sample (Figure 26). The features that are characteristic of CLFM, movement away from the center of curvature, formation of a new solid solution, and reversals of curvature, were not observed. Therefore, it was difficult to confirm whether CLFM occurred at this temperature. The system begins to equilibrate at 1260°C. This is evident since the grains and grain boundaries appear to be approaching an equilibrium shape. If CLFM occurs at all at 1260°C, it happens so quickly that it is difficult to observe.

5. Similar Features of CLFM and DIGM:

The movement of grain boundaries away from their centers of curvature, the formation of alloyed or dealloyed zones on the concave side of the migrated boundary, and the presence of reversals of curvature along the grain boundary are also characteristic of DIGM. However, Radhakrishnan (37) showed experimental evidence that the migration observed in alloy 718 occurred with the boundary in the liquid state. Radhakrishnan made several observations in the weld HAZ to show that the phenomenon observed was CLFM instead of diffusion induced

grain boundary migration (DIGM). Recall that DIGM is the phenomenon where grain boundaries migrate as a result of solute atoms diffusing along the grain boundaries (1,2,3,4).

The following observations were made by Radhakrishnan (37) to show that the observed phenomenon in the weld HAZ of alloy 718 was CLFM:

- 1) Samples heated to peak temperatures of 1200°C and 1215°C revealed the presence of migration. These temperatures are above the carbide liquation temperature for the as-received, the homogenized, and aged alloys.
- 2) Examination of a Spot Varestraint Test specimen showed that a boundary neighboring one of the HAZ cracks exhibited migration identical to the migration observed at a peak temperature of 1200°C. It is known for alloy 718 that the hot cracks are produced by the presence of a grain boundary liquid.
- 3) The dissolution of the carbides at a heat treatment temperature of 1093°C did not result in DIGM. Also, the dissolution of the δ -phase and NbC at a peak temperature of 1175°C does not result in any DIGM. This shows that the migration process did not first occur as a result of DIGM, due to the dissolution of carbides along grain

boundaries, and that the liquation process did not occur after the DIGM process.

The observations by Radhakrishnan are also applicable to the alloy 718 used in the present study. The experimental observations of Radhakrishnan showing that the migration process started in the presence of liquid are similar to observations made in the present study. These observations, along with those presented here, confirm that the migration observed in the alloy 718 of the present study occurred with the boundary in the liquid state.

B. Niobium Concentration Versus Temperature

There were no standards used in the TEM/EDS analysis for determining the semi-quantitative values of the niobium concentration. The relative differences between the niobium concentrations in the matrix and the migrated region were of primary concern, not the actual semi-quantitative values. The semi-quantitative values of niobium concentration were plotted as a function of distance (Figures 13, 19, 20, 21, and 25) to illustrate the relative differences between the niobium concentrations in the matrix and the migrated region.

The concentration of niobium in the migrated region was higher than the niobium concentration in the matrix for the 1227°C for 4 seconds thermal cycle. The niobium concentration

was determined to be approximately 1.5 times higher in the migrated region than in the matrix. Temperatures below the solidus temperature but above the eutectic temperature for this alloy should result in a higher niobium concentration than that determined by the alloy composition. Since 1227°C falls within this range, the niobium concentration was expected to be higher in the migrated region than in the matrix.

The higher niobium concentration in the migrated region can be explained using the approximate γ -NbC pseudo-binary phase diagram shown in Figure 30. This pseudo-binary phase diagram was constructed from the data shown in Table VIII that was obtained from early work on alloy 718 involving the physical metallurgy of this alloy system (32). Table VIII also shows data obtained from work on the solidification diagram of alloy 718 (31) and from work on the solidification of grain boundary liquid in the HAZ of alloy 718 (27). The maximum solid solubility of niobium in the matrix shown in Figure 30 (9.6 wt.%) is the average of the values that were reported by Knorovsky et al. (31) and Radhakrishnan and Thompson (27). The γ -NbC eutectic temperature (1176°C) shown in Figure 30 is the average value of the data reported by Eiselstein (32) and

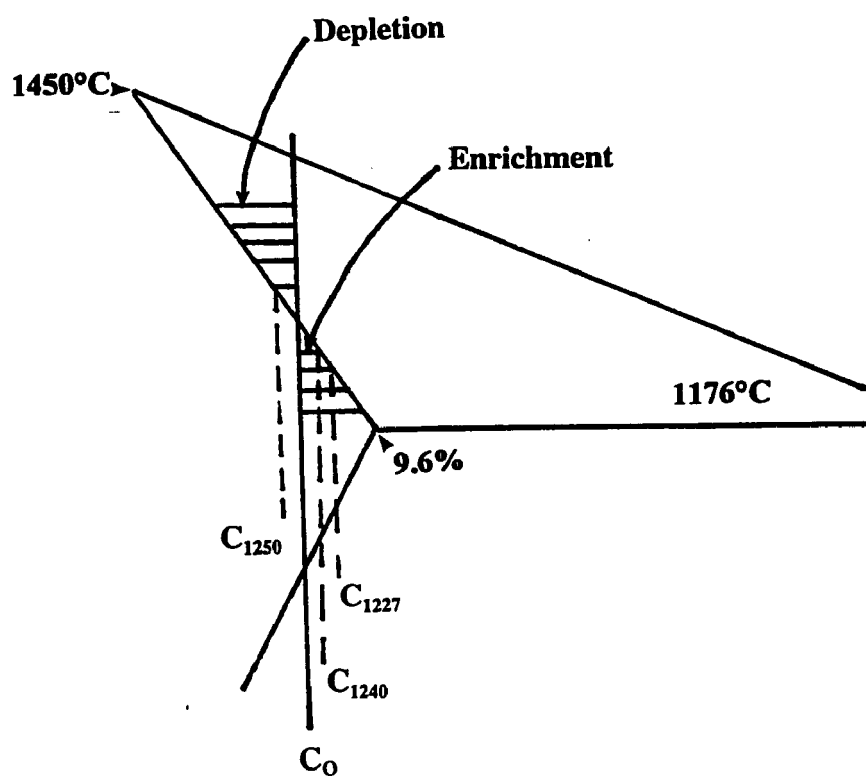


Figure 30. Approximate γ -NbC pseudo-binary phase diagram showing compositions of niobium for 1227°C , 1240°C , and 1250°C .

Radhakrishnan and Thompson (27). The melting point of γ was taken from Radhakrishnan and Thompson (27).

The composition of the alloy 718 that was used in the Radhakrishnan and Thompson (27) study was similar to the alloy 718 composition used in the present study. Therefore, the data from Radhakrishnan and Thompson (27) was used with the data from Knorovsky et al. (31) to determine the average value of the maximum solid solubility of niobium in the matrix and it was combined with the data from Eiselstein (32) to determine the average γ -NbC eutectic temperature. The Radhakrishnan and Thompson (27) study was inspired by previous CLFM work by these authors (23,37) that is similar to the alloy 718 CLFM work of the present study. Therefore, the reported values of the melting point of γ from the Knorovsky et al. (31) and Eiselstein (32) studies were not used in constructing the pseudo-binary phase diagram in Figure 30.

If the tie-line is drawn for 1227°C, the corresponding composition of niobium for this temperature is denoted by C_{1227} in Figure 30 which is the composition where the tie line intersects the γ solidus curve. As shown on the pseudo-binary diagram, C_{1227} is greater than the niobium concentration of the matrix that is denoted by C_0 . Hence at 1227°C, enrichment of the migrated zone occurred which signifies that this

temperature is below the solidus temperature of this alloy. As shown in Figure 10, the appearance of the microstructure for the 1227°C sample helps confirm that this temperature is below the solidus temperature. This is evident since there appears to be no melting in the matrix at this temperature. The measured semi-quantitative value of niobium concentration in the migrated region was determined to be approximately 9.4 wt.%. This falls within the range of maximum solid solubility of niobium in the matrix values (7-10 wt.%) that were obtained from the literature (Table VIII).

The 1240°C sample also had niobium segregation in the migrated region. The niobium concentration in the migrated region was determined to be approximately 1.5 times greater than the niobium concentration in the matrix. This niobium enrichment can also be explained using the γ -NbC pseudo-binary phase diagram in Figure 30. If the tie-line is drawn for this temperature, the corresponding concentration of niobium is denoted by C_{1240} . As shown on the pseudo-binary phase diagram, C_{1240} is greater than C_0 but less than C_{1227} . This is in agreement with the results of the present study. The average composition of niobium in the migrated region for the 1240°C sample was determined to be 8% which is greater than the alloy composition of 5.05%.

Table VIII. Data for Construction of γ -NbC Pseudo-Binary Phase Diagram

	Eiselstein (ref. 32)	Knorovsky (ref. 31)	Radhakrishnan (ref. 27)
Maximum Solid Solubility of Niobium (wt. %)	7	9.3	10
γ -NbC Eutectic Temperature (°C)	1177	1198	1175
Melting Point of γ (°C)	1360	1410	1450

The microstructure for the 1240°C sample in Figure 16 shows that there appears to be no melting of the matrix at this temperature. This suggests that 1240°C is also below the solidus temperature for this alloy. Therefore, niobium enrichment was expected to occur in accordance with the pseudo-binary phase diagram for γ -NbC.

The 1250°C sample did not show niobium enrichment in the migrated region. There was no significant difference between the niobium concentration in the migrated region and the niobium segregation in the matrix. However, observation of the niobium concentration versus distance plot for this temperature (Figure 25) shows that the niobium concentration appears to decrease slightly upon approaching the migrated grain boundary (denoted as liquid film). Once across the migrated grain boundary, the niobium concentration starts off slightly low then it increases to an approximately uniform value in the matrix.

It was expected that the migrated region would be depleted of niobium since 1250°C is believed to be above the solidus temperature for this alloy. The pseudo-binary phase diagram in Figure 30 shows that the tie-line for 1250°C corresponds to a niobium concentration denoted by C_{1250} which is less than the alloy composition, C_0 , and is also less than

C_{1227} and C_{1240} . This is in agreement with the results of the present study. The average concentration of niobium in the migrated region for the 1250°C sample was determined to be 4.2% which is less than the niobium concentrations that were determined for the 1227°C and 1240°C samples.

Earlier work of LFM in alloy 718 by Radhakrishnan and Thompson (23) can be used to help explain the observation of uniform niobium concentration across the migrated region and matrix at 1250°C instead of niobium depletion in the migrated region that was expected. Radhakrishnan and Thompson showed that migration occurred at very short times such as 1 second at 1200°C. In the present study, the samples were heated at a rate of 100°C per second to 1200°C. In order to heat at the same rate from 1200°C to the various peak temperatures used in this study, the difference in temperature between 1200°C and the peak temperature was divided by 100°C and multiplied by 1 second. For example, the heating rate for the 1250°C thermal cycle consisted of 100°C per second to 1200°C then 50°C per 0.5 second to 1250°C.

Since Radhakrishnan and Thompson (23) observed migrated boundaries after a 1 second hold at 1200°C, it is believed that in the present study some migration could have occurred during the heating time from 1200°C to the peak temperature

1250°C in addition to the migration occurring after a 4 second hold at 1250°C. If migration did occur during the heating time from 1200°C to 1250°C, this could explain the uniform niobium concentration across the migrated region and the matrix. It is possible that most of the migration occurred during the heat up from approximately 1200°C to 1250°C. While the sample was being held for 4 seconds at this temperature, there may have been little migration occurring. This could have resulted in a significant amount of time for the niobium in the matrix to diffuse into the migrated region thus causing the niobium concentration in the matrix and the migrated region to be similar. The observation of uniform niobium concentration across the migrated region and matrix also suggests that the system is beginning to equilibrate at 1250°C.

The microstructure of 1250°C shown in Figure 22 shows evidence of melting in the matrix that is characteristic of being above the solidus temperature. There are many small particles dispersed throughout the matrix at this temperature. These particles resulted due to the solidification of the niobium rich liquid that formed in the matrix when the temperature was raised above the solidus temperature and into the two phase γ + Liquid region of the phase diagram. TEM/EDS analysis showed that these particles were niobium rich. By

comparing the microstructures for 1227°C (Figure 10) and 1240°C (Figure 16) to the microstructure for 1250°C (Figure 22), it is quite evident that these particles are not present in the matrix for 1227°C and 1240°C. It is also evident that the microstructures for 1227°C and 1240°C are somewhat similar to each other but are not similar to the microstructure for 1250°C. These observations support the theory that 1227°C and 1240°C are below the solidus temperature and that 1250°C is above the solidus temperature.

As stated earlier, it was difficult to determine the original grain boundary position in the 1260°C sample because it was indistinguishable from the matrix. Therefore, the niobium concentration was not determined for the 1260°C sample. If CLFM occurred at all at 1260°C, it could have happened so quickly that it was difficult to observe. It is also possible that the original grain boundary position could not be determined because CLFM was suppressed at 1260°C. Kim and Yoon (38) showed that LFM was suppressed at high temperatures in a Co-Cu alloy. They showed that at high temperatures and low driving forces, coherency breaking could occur in the region located in front of the migrating grain boundary (frontal diffusion zone).

The results for the 1227°C, 1240°C, and 1250°C samples help prove the theory of niobium segregation that was proposed for this study. The theory is that the concentration of niobium in the migrated region will follow the solidus curve of the phase diagram for this alloy. This will result in reversed niobium segregation as the peak temperature is raised above the solidus temperature. This theory was based on the γ -NbC pseudo-binary phase diagram. As the temperature is increased, the niobium concentration should follow the solidus curve and decrease as a function of increasing temperature. The results for 1227°C, 1240°C and 1250°C showed that this did occur. The niobium concentration in the migrated region decreased as the peak temperature was increased from 1227°C to 1250°C.

C. Migration Rate Versus Temperature

The migration rate was shown to increase only slightly from 1227°C to 1240°C and there was no increase in migration rate from 1240°C to 1250°C as shown in Figure 29. The migration rate appeared to reach a maximum value at 1240°C. This observation is consistent with the coherency strain theory that predicts a high temperature limit, above which, LFM does not occur. The fact that CLFM was observed for 1250°C

but not for 1260°C can possibly be explained with help from the coherency strain theory.

Kim and Yoon (38) stated that coherency breaking occurs when the ratio of the solute diffusivity to the migration velocity becomes very large at high temperatures thus, eliminating LFM. Kim and Yoon expressed the condition for coherency breaking in the region in front of the migrating grain boundary (frontal diffusion zone) as

$$l_c = \frac{D}{v}$$

In the present study, a similar criterion was used to predict coherency breaking which results in the suppression of CLFM. The criterion was based on the equation for coherency breaking that was defined by Kim and Yoon (38) which consisted of the ratio of the solute diffusivity to the migration velocity. The niobium diffusivity was divided by the migration rate (D/MR) for each temperature in the present study. These values, shown in Table IX, increased as a function of increasing temperature from 1227°C and 1260°C. CLFM was observed at 1227°C, 1240°C, and 1250°C but not at 1260°C. Coherency breaking probably occurred in the frontal diffusion zone of the 1260°C sample which resulted in the suppression of CLFM at this temperature. According to the criterion for

Table IX. Diffusivity/Migration Rate (D/MR) Values

Temperature (°C)	D/MR (cm)
1227	7.924×10^{-5}
1240	8.937×10^{-5}
1250	10.32×10^{-5}
1260	12.03×10^{-5}

coherency breaking, CLFM should be suppressed for large D/MR values. Therefore, the large D/MR value for 1260°C can be used to explain why suppression of CLFM occurs at this temperature. These observations support the belief that CLFM was suppressed at 1260°C.

The steady state migration velocity was shown by Brecht and Purdy (28) to be

$$v = \frac{12\sigma D_L}{5L^2} \left(\frac{4C_o}{C_L \bar{k}L} - 1 \right)$$

where σ is the solid-liquid interfacial energy, D_L is the diffusion coefficient for solute in the liquid, L is the length of the liquid film, C_o is the solute concentration of the matrix in the growing grain, C_L is the solute concentration in the liquid at the trailing interface, and \bar{k} is the average curvature of the liquid film.

This equation shows that there are other possible mechanisms for slowing or stopping the migration process. Since the above equation shows that the migration velocity is directly proportional to D_L , a low value for this term would result in a slower migration velocity. Also, the migration velocity would decrease as the length of the liquid film increases since the velocity is inversely proportional to the

square of the length of the liquid film (L^2). Therefore, CLFM can also be suppressed when the diffusivity of the solute in the liquid is very low or as the liquid film grows.

D. Influence of Crystal Orientation on CLFM

Since all of the 90 pairs of grains were separated by CLFM boundaries, this result showed that CLFM can occur over a large range of orientations. It can also be seen from this result that NbC precipitates can liquate and cause wetting along grains of different orientations (29).

The migrated grain boundaries were examined in order to determine if the orientation of the grain had an effect on the direction which the grain boundary migrated. From the observation of migration on both sides of the boundary, the crystal orientation does not restrict the migration direction (29).

Previous researchers showed that the coherency strain was directly proportional to the orientation dependent modulus for a given solute (14). Since the results of the present study show that the crystal orientation did not restrict the migration direction, the coherency strain hypothesis can not be used exclusively to explain the driving force for CLFM that was observed for alloy 718. As stated previously, the CLFM observed in the present study originated from discrete

precipitates which produce the in-plane solute flux as found in DIGM and as necessary to operate the Brechet and Purdy (28) model for LFM. Therefore, the in-plane solute flux theory must also be considered as a possible driving force for the migration that was observed in this study.

SUMMARY

1. CLFM was confirmed for 1227°C, 1240°C and 1250°C by the following observations: (a) the grain boundaries moved away from their centers of curvature, (b) the formation of a new solid solution behind the migrated grain boundaries, and (c) the reversals of curvature of the migrated grain boundaries.
2. Niobium enrichment or depletion in the region behind the migrated grain boundary appeared to follow the solidus curve as predicted by an equilibrium solid-liquid interface.
3. The migration rate increased with increasing temperature but appeared to reach a maximum value above the solidus temperature.
4. CLFM was suppressed at 1260°C.
5. NbC precipitates were shown to liquate and cause wetting along grains of all orientations.

CONCLUSIONS

1. The theory that solute concentration in the region behind the migrated liquid film would follow the phase diagram solidus was verified affirmatively. This shows that the solid-liquid interface can be treated as an equilibrium interface.
2. The behavior of the migration rate with increasing temperature suggests that migration becomes suppressed at high temperatures. This is consistent with the coherency strain theory that predicts a high temperature limit for LFM.
3. CLFM can occur in a large number of crystal orientations as evidenced by the migration seen on both sides of the grain pairs.

LIST OF REFERENCES

1. M. S. Sulonen: Acta Metall., 1960, vol. 8, pp. 669-76.
2. F. J. A. Den Broeder: Acta Metall., 1972, vol. 20 pp.319-32.
3. M. Hillert and G. R. Purdy: Acta Metall., 1978, vol. 26, pp.333-40.
4. R. W. Balluffi and J. W. Cahn: Acta Metall., 1981, vol. 29, pp.493-500.
5. D. N. Yoon: Annual Review of Materials Science, 1989, vol. 19, pp.43-58.
6. D. N. Yoon and W. J. Huppmann: Acta Metall., 1979, vol. 27, pp.973-77.
7. Y. Song, S. Ahn, and D. N. Yoon: Acta Metall., 1985, vol. 33, pp. 1907-10.
8. M. Hillert: Scripta Metall., 1983, vol. 17, pp. 237-40.
9. C. A. Handwerker: in Diffusion Phenomena in Thin Films and Microelectronic Materials, D. Gupta and P. S. Ho eds., Noyes Publications, Park Ridge, NJ, 1987, pp. 245-322.
10. D. A. Porter and K. E. Easterling: Phase Transformations in Metals and Alloys, New York, 1992, pp. 44-45.
11. D. A. Porter and K. E. Easterling: Phase Transformations in Metals and Alloys, New York, 1992, pp. 154-155.
12. M. Hillert: Metall. Trans., 1972, vol. 3, pp. 2729-41.
13. T. Muschik, W. A. Kaysser, and T. Hehenkamp: Acta Metall., 1989, vol. 37, pp. 603-13.

14. J. W. Cahn: Acta Metall., 1961, vol. 9, pp. 795-801.
15. B. Radhakrishnan and R. G. Thompson: A Proposal to the Department of Energy, 1990.
16. Y. J. Baik and D. N. Yoon: Acta Metall., 1985, vol. 33, pp. 1911-17.
17. Y. J. Baik and D. N. Yoon: Acta Metall., 1986, vol. 34, pp. 2039-44.
18. W. H. Rhee, Y. Song, and D. N. Yoon: Acta Metall., 1987, vol. 35, pp. 57-60.
19. W. H. Rhee and D. N. Yoon: Acta Metall., 1987, vol. 35, pp. 1447-51.
20. W. H. Rhee and D. N. Yoon: Acta Metall., 1989, vol. 37, pp. 221-28.
21. Y. J. Baik and D. N. Yoon: Acta Metall., 1990, vol. 38, pp. 1525-34.
22. M. Kuo and R. A. Fournelle: Acta Metall., 1991, vol. 39, pp. 2835-45.
23. B. Radhakrishnan and R. G. Thompson: Scripta Metall., 1990, vol. 24, pp. 537-42.
24. B. Radhakrishnan and R. G. Thompson: Metall. Trans. A, 1993, vol. 24A, pp. 2773-85.
25. R. Nakkalil, N. L. Richards, and M. C. Chaturvedi: Scripta Metall., 1992, vol. 26, pp. 1599-1604.
26. R. Nakkalil, N. L. Richards, and M. C. Chaturvedi: Acta Metall., 1993, vol. 41, pp. 3381-92.
27. B. Radhakrishnan and R. G. Thompson: Metall. Trans. A, 1992, vol. 23A, pp. 1783-99.
28. Y. Brechet and G.R. Purdy: Scripta Metall., 1988, vol. 22, pp. 1629-33.

29. V. L. Acoff, R. G. Thompson, and R. D. Griffin: in Proceedings of Solid - Solid Phase Transformations Conference, 1994.
30. B. Radhakrishnan and R. G. Thompson: Metall. Trans. A, 1991, vol. 22A, pp. 887-902.
31. G. A. Knorovsky, M.J. Cieslak, T.J. Headley, A.D. Romig, and W.F. Hammetter: Metall. Trans. A, 1989, vol. 20A. pp. 2147-58.
32. H. L. Eiselstein: Advances in the Technology of Stainless Steels, ASTM STP 369, 1965, pp. 62-79.
33. B. R. Patterson: Personal Communication.
34. V. Randle: The Measurement of Grain Boundary Geometry, Institute of Physics Publishing, Bristol, UK, 1993, pp. 104-105.
35. Y. J. Baik and D. N. Yoon: Acta Metall., 1987, vol. 35, pp. 2265-71.
36. Z. Guan, G. Liu, and J. Du: Acta Metall., 1993, vol. 41, pp. 1293-1300.
37. B. Radhakrishnan: Ph.D. Dissertation, The University of Alabama at Birmingham, Birmingham, Alabama, 1989.
38. J. K. Kim and D. Y. Yoon: Acta Metall., 1994, vol. 42, pp. 913-19.

APPENDIX

DERIVATION OF σ_T

$$\sigma_A = \frac{\sigma_T}{\cos \phi}$$

or

$$\frac{1}{\sigma_A} = \frac{\cos \phi}{\sigma_T}$$

$$\left(\frac{1}{\sigma_A} \right) = \left(\frac{1}{\sigma_T} \right) \int_0^{\frac{\pi}{2}} \cos \phi [f(\phi) d\phi]$$

where $[f(\phi) d\phi]$ is probability of orientation in range $d\phi$

$$f(\phi) d\phi = \frac{d\phi}{(\pi/2)}$$

$$\left(\frac{1}{\sigma_A} \right) = \left(\frac{1}{\sigma_T} \right) \left(\frac{2}{\pi} \right) \int_0^{\frac{\pi}{2}} \cos \phi d\phi$$

$$\left(\frac{1}{\sigma_A} \right) = \left(\frac{2}{\pi \sigma_T} \right) [\sin x]_0^{\frac{\pi}{2}}$$

$$\left(\frac{1}{\sigma_A} \right) = \left(\frac{2}{\pi \sigma_T} \right) [1 - 0]$$

$$\left(\frac{1}{\sigma_A} \right) = \left(\frac{2}{\pi \sigma_T} \right)$$

$$\sigma_T = \frac{2}{\pi} \left(\frac{1}{\left(\frac{1}{\sigma_A} \right)} \right) = 0.64 \left(\frac{1}{\left(\frac{1}{\sigma_A} \right)} \right)$$

GRADUATE SCHOOL
UNIVERSITY OF ALABAMA AT BIRMINGHAM
DISSERTATION APPROVAL FORM

Name of Candidate Viola L. Acoff

Major Subject Material Science and Engineering

Title of Dissertation An Analysis Of Constitutional Liquid Film

Migration In The Nickel-Base Alloy 718

Dissertation Committee:

Raymond C. Thompson, Chairman

Robin D. Griffith

Barton D. Patterson

Benny Andrews

John Ford

Director of Graduate Program

J. M. Rogers

Dean, UAB Graduate School

Jean P. Losh

Date 12/1/94